School of Electrical and Electronic Engineering
Sackville Street Building
Sackville Street
University of Manchester
Manchester
M13 9PL
tel+44(0)161 306 9340
www.manchester.ac.uk/EEE

Dynamic Thermal Modelling of Low Voltage Underground Cables

Deliverable 2

Prepared for Dr Geraldine Bryson (Electricity North West)

Prepared by Martin Caton, Ognjen Marjanovic and Simon Rowland (University of Manchester)

Date: 14/07/2015

Table of Contents

Executive Summary

This report details the results of the project funded under IFI that focused on dynamic thermal modelling of low-voltage underground cables. Also, the emphasis was on understanding and quantifying the thermal inertia present in the underground cable that prohibits instantaneous changes in cable temperature and may be utilised to absorb short-term high-amplitude bursts of current without causing excessive temperature rise inside the cable.

The cable considered in this study was Prysmian Waveform cable that was modelled using a high-fidelity Finite Element Analysis approach. The resultant model was subjected to a number of numerical experiments in order to better understand the dynamic thermal behaviour of the underground cable and the impact of various environmental factors such as moisture content in the soil and seasonal changes in ambient temperature.

The methodology of modelling a real LV network was presented and it was shown how the impact of incorporating low-carbon technologies on the thermal behaviour of the cables can be assessed in order to inform future network design as well as future operational considerations, such as demand side management (DSM). In particular, the impact of integration of electric vehicles (EVs) on the cable temperature was demonstrated. Also, it was shown how the modification of a charging schedule that introduces a synchronised duty cycle can allow significant increase in the penetration level of EVs that does not violate thermal constraint.

A thermal model was also evaluated using pulse response experiments which provided a useful insight into thermal behaviour of the cable when the sudden changes in load occur. These experiments were also conducted with different soil moisture content levels and ambient temperature to reflect seasonal changes. The key observation from these numerous simulations was that the dry soil conditions significantly increased the temperature experienced inside the cable and therefore reduced the current carrying capacity of the cable. The impact of seasonal changes on ambient temperature had a much smaller, linear and directly proportional impact on the cable temperature.

The relationship between cable temperature and current observed during the pulse response experiments was utilised to derive simplified dynamic thermal models of the LV waveform cable. This simplified model is implemented using the Microsoft Excel software package and allows user to specify initial cable loading and the step change in the cable current as well as the ambient temperature in order to observe cable temperature time-profiles for three different soil moisture content levels.

1 Introduction

1.1 Background

Underground (UG) low voltage (LV) cables have high economic value owing to their abundance in urban distribution networks (DNs) and the costs associated with their installation and/or replacement. These cables are owned by distribution network operators (DNOs) who are responsible for their installation, management, configuration, maintenance and replacement.

One of the key challenges facing DNOs today is a significant change in the electric power flow arising from increased penetrations of electric vehicles (EVs), heat pumps (HPs) and photo voltaic micro generation (PV). Urban areas of the UK's LV DN is where the majority of these loads and generators will be connected and it is also an area that is presently heavily loaded during winter months. It has been shown that 10% to 20% market penetration of EVs alone would lead to an 18% to 36% increase in the daily peak demand placed on the LV DN [1]. This effect is compounded by the recorded increase of 16,542% in domestic generation in the three years leading up to January 2013. These evolving changes will significantly alter the existing power flow, which is expected to increase instances of thermal distributor overload and invoke premature aging induced by higher operating temperatures.

A greater understanding of the thermal behaviour exhibited by UG LV distributors could be used by DNOs to maximise their lifetime by applying this new understanding to network design, maintenance and asset management procedures. In particular, understanding the extent and impact of thermal inertia present in UG distributors may prove to be critical in determining their optimal capacity utilisation.

The presence of thermal inertia prevents temperatures inside a cable from responding instantaneously to changes in its conductor currents. Therefore, short term overloading of the underground cables could possibly be tolerated by exploiting the presence of thermal inertia. However, it is necessary to develop sufficiently accurate thermal models that capture the relationship between a cable's conductor current and the resultant maximum cable temperature in order to be able to fully utilise thermal inertia. These dynamic thermal models would have to be able to predict cable temperatures over time when provided with time varying conductor current profiles and be accessible through a software package readily available to DNO network designers. Also, these models could be used to determine current profiles that maximise cable capacity, whilst ensuring that the thermal constraints are not violated.

1.2 Objectives

The key objective of the work described in this report was the development of a high-fidelity dynamic thermal model that is capable of predicting cable temperature for a given cable current and ambient temperature.

An additional objective was to identify a simple model that sufficiently approximates a high-fidelity dynamic thermal model but that does not rely on a complex proprietary software package in order to allow a network designer to estimate cable temperature for various current profiles.

The final objective was to improve the understanding of the dynamic thermal behaviour of underground cables and, in particular, investigate its dependence on factors such as thermal properties of the soil and ambient temperature.

1.3 Outline of the Report

This report is structured as follows. Chapter 1 provides background information for the project, lists the main objectives and outlines the structure of the report. Chapter 2 initially reviews the standard approach used in industry to perform thermal rating of the cables and then details development of the high-fidelity dynamic thermal model of the LV waveform cable. Chapter 3 documents numerical experimental results obtained by evaluating a high-fidelity thermal model of the LV waveform cable. These model evaluations include response of cable temperature to sudden changes in cable current and also the ability to incorporate an electrical model of a given real-world LV network with the dynamic FEA model to estimate the cable temperature inside the actual LV feeder. Chapter 4 briefly introduces a simplified dynamic thermal model of the LV waveform cable that has been implemented using a Microsoft Excel software package. Finally, concluding remarks are drawn in Chapter 5.

2 Thermal Modelling of the Underground LV Cable

This chapter describes the development of a high fidelity dynamic thermal model that was designed to capture the relationship between cable current and temperature over time. Initially, the standard IEC models that are used in the present day by manufacturers and DNOs to thermally rate cables are outlined. Then the details regarding the development of a high-fidelity dynamic thermal model based on Finite Element Analysis (FEA) is described along with some design considerations such as the resolution of the FEA mesh used in the thermal model and the sizing of the surrounding medium required to replicate the behaviour of cables deployed in the outside environment.

2.1 Review of the Existing Thermal Rating Standards

The operational thermal capacity of underground power cables is typically evaluated by applying IEC 60287 [2] which specifies the standard cable model shown in Figure 1 that relates phase conductor temperature to an ampacity rating. In the standard, the rise of cable temperature above ambient temperature is denoted as $\Delta\theta$ which is defined as being related to the cable construction parameters featured in equation (1) where R is the alternating current resistance of a conductor at its maximum operating temperature (Ω/m), W_d represents the dielectric losses per unit length per phase (W/m), W_A represents the losses in armour per unit length (W/m), W_s represents the losses dissipated in sheath per unit length (W/m), $\lambda_1$and λ_2 are the ratios of the total losses in metallic sheaths and armour respectively to the total conductor losses, and finally T_1 to T_4 denote thermal resistance per core between conductor and sheath, thermal resistance between sheath and armour, thermal resistance of external serving and the thermal resistance of surrounding medium, respectively (K.m/W).

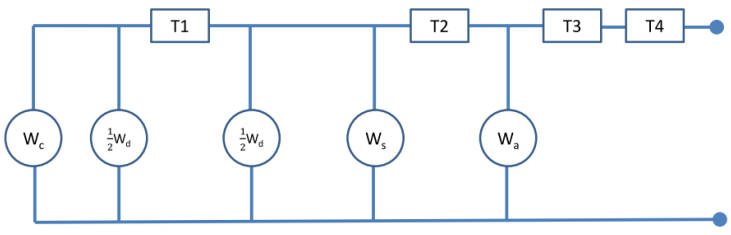

Figure 1: IEC 60287 Standard Cable Model

$$\Delta\theta = \left(I^2R + {}^1/_2\, W_d\right)T_1 + [I^2R(1+\lambda_1) + W_d]nT_2 + [I^2R(1+\lambda_1+\lambda_2) + W_d]n(T_3+T_4) \quad (1)$$

Equation (1) can be rearranged in order to calculate the rms phase conductor current rating of a cable for a given rise of cable temperature above ambient temperature:

$$I = \left[\frac{\Delta\theta - W_d[0.5T_1 + n(T_2+T_3+T_4)]}{RT_1 + nR(1+\lambda_1)T_2 + nR(1+\lambda_1+\lambda_2)(T_3+T_4)}\right]^{0.5} \quad (2)$$

The IEC standard is used by cable manufacturers to provide a rating value for a cable's current carrying capacity which they then certify through a laboratory test. In the UK, BS 7870 [3] specifies the laboratory tests which consist of heating cables whilst they are mounted under water and in the air. During these tests, cable heating is induced by passing a balanced electrical current through its phase conductors while a thermocouple monitors the cable's sheath temperature and the resistance of its phase conductors is recorded. The conductor temperature is then estimated using the IEC model parameters and the sheath temperature measurement. Verification of this conductor temperature estimate is performed using the electrical resistance readings and look up tables that relate it to conductor temperature. The heating cycles are restricted in time to eight hour durations, whereby two hours is allocated to the maintenance of the conductor temperature between 5°C and 10°C above the rated temperature, and three hours to natural cooling. Both the soil resistivity and ambient temperature values that were assumed in the manufacturers rating calculation are specified in the relevant cable manufacturer's data sheet.

DNOs also use the IEC standard 60827 to rate the cables that they purchase and own in order to evaluate their capacity in the context of the conditions in which they are required to operate. The main parameters that are different to those that cable manufacturers use are soil resistivity and ambient temperature, which are discussed in the following two paragraphs respectively.

Particular guidance is provided in the IEC standard on specific values of soil resistivity to use, which it notes as being dependent upon soil moisture content, country and climate. For the UK, a soil resistivity of 1.2 K.m/W is suggested in the IEC standard, although it also separately notes that the thermal resistivity of soil could be 0.7 K.m/W when very moist and 3 K.m/W when very dry. The ENA (Energy Networks Association) Engineering Recommendation P17 [4] provides another value of soil resistivity, which is 0.9 K.m/W and used by DNOs when rating cables destined for installation on their networks. A review of this ENA document has recently been conducted by NPG (Northern Power Grid) and EA Technology as part of the CLNR (Customer Lead Network Revolution) project [5].

It found that at the sites where soil conductivity was measured, soil resistivity was calculated as being 1.5 K.m/W in the summer and 2 K.m/W in the winter. The actual value of soil resistivity that is used by ENW and some other UK DNOs to evaluate current ratings when designing new cable networks is the ENA value of 0.9K.m/W. However, the NPG review [5] highlights the discrepancy between the ENA value for soil resistivity and the actual values that were derived from the thermal conductivities measured over the course of the RTTR (real-time thermal rating) trial [6]. Also, it notes that these values indicate that if the IEC standard method and ENA value for soil resistivity is used, cables should be de-rated by 10% in the winter and 16% in the summer.

According to the NPG review, the ENA recommends using an ambient soil temperature of 10^{o}C to determine the winter rating and 15^{o}C to calculate the summer rating. However, the CLNR project measured maximum temperatures of 17^{o}C in summer and 8^{o}C in winter which leads to the conclusion that there may be a case to increase the assumed summer value above 15^{o}C in areas that experience peak load at this time.

Cable rating calculations by most DNOs are applied through the CRATER software package which is licenced to them by EA Technology and uses the standards to provide a continuous and cyclic cable rating for a given set of parameters. Continuous cable ratings can be found by applying IEC 60827 whilst cyclic ratings can be calculated using a loss-load cycle which is a look up table of the percentage of maximum load that is carried by the cable in the hours that precede its maximum conductor temperature. A methodology for calculating cyclic and emergency cable ratings is provided in the IEC standard 60853.

2.2 Dynamic Thermal Model Development

The main critique of the thermal rating methods currently used is the fact that they mostly ignore the presence of thermal inertia which may have significant impact, particularly during normal, non-emergency but possibly significant temporal variations in the load. This has become particularly relevant in recent years with the introduction of novel low-carbon technology loads, such as electric vehicles, electric heaters and heat pumps that may cause significant changes in temporal variation of load patterns experienced by the low voltage underground cables. Therefore, it becomes important to more thoroughly understand how the cable current affects its temperature for various scenarios beyond rather restrictive quasi-steady-state considerations that are in current practice.

In order to understand and then fully exploit the presence of thermal inertia, a high-fidelity dynamic thermal model of the underground LV cable needs to be developed, details of which are provided in this section.

2.2.1 Physical Layout of the LV Waveform Cable

Work documented in this report was concerned with thermal modelling of LV waveform cable, which is widely used by DNOs. A pictorial view of the LV waveform cable is shown in Figure 2.

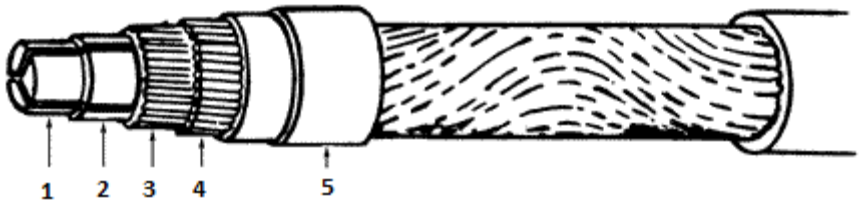

Figure 2: Pictorial view of an LV waveform cable

A cross sectional view of the same LV waveform cable is shown in Figure 3.

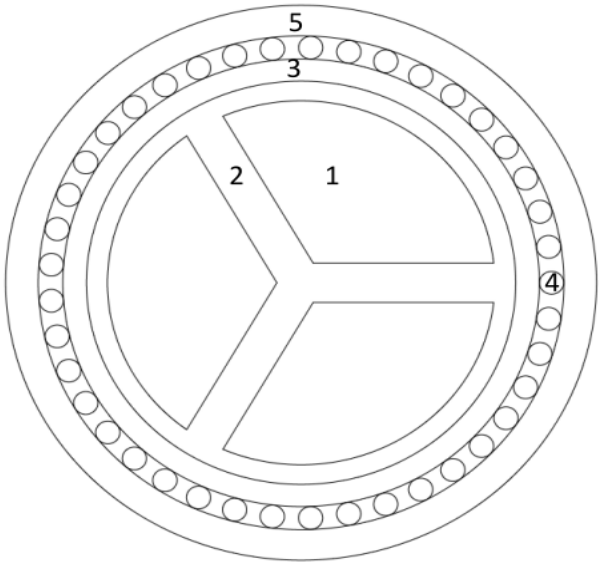

Figure 3: Cross sectional view of an LV waveform cable

The five components of the LV waveform cable shown in Figure 2 and Figure 3 are defined in the Table 1.

Table 1: The five components of an LV waveform cable

Label used in Figure 2 and Figure 3	Component Description
1	solid aluminium conductors
2	XLPE core insulation
3	rubber anti-corrosion bedding
4	aluminium wires surrounded with rubber anti-corrosion bedding
5	extruded PVC over-sheath

The inner dimensions for the LV waveform cable were determined using manufacturer's data sheets and the British Standards that the cables were manufactured to comply with. All the physical measurements are defined in Figure 4 and their values are given in Table 2.

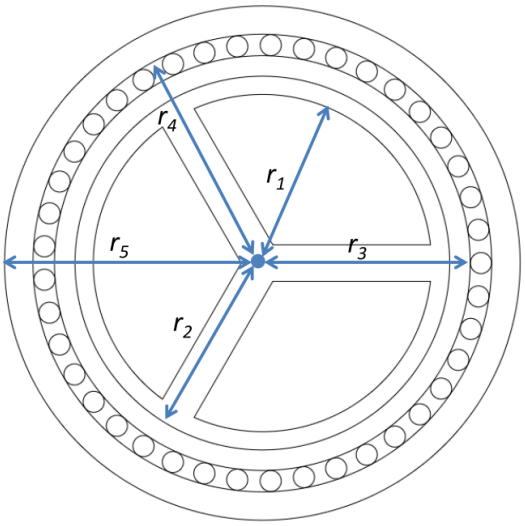

Figure 4: Physical measurements of 185 mm^2 Prysmian Waveform cable

Table 2: Measurements labelled in Figure 4

Measurement Label	Length (mm)
r_1	14.81
r_2	16.41
r_3	18.21
r_4	20.09
r_5	22.58

2.2.2 Development of The High Fidelity Dynamic FEA Thermal Model

Finite Element Analysis (FEA) attempts to numerically solve the complicated physics-based problems that may exhibit complex spatial as well as temporal variations. In the context of thermal modelling of the underground cable, FEA breaks down the spatial representation of a modelled system into a large number of small, ideally infinitesimal, regions, denoted as nodes, each of which exchanges heat with the adjacent nodes through mutual thermal resistance and each of the nodes having associated with them thermal capacity. The particular software package used in this project to create and then evaluate developed FEA models is COMSOL Multiphysics®.

To create a COMSOL model a two dimensional cross-sectional CAD drawing of a cable is created and then placed inside the square shaped area representing the surrounding medium, e.g. soil. Within the drawing, each unique feature which could be a conductor or a concentric insulator layer inside the cable or the surrounding medium is represented as an individual CAD object.

Figure 5 contains an example of a labelled CAD drawing used to create a model which is a 185 mm^2 Prysmian Waveform cable placed in a square shaped area which represents the surrounding medium. Each unique object in the figure is labelled using either a *h* or an *m* to denote a heat source or a physical material respectively. The red line in the figure is used to indicate that the ground surface is modelled as a temperature source, denoted as T_A, and represents the ambient ground surface temperature. The fact that the ground surface is modelled as a temperature source implies that T_A is assumed to be an independent variable and is unaffected by the thermal behaviour of the cable or its surrounding medium. On the other hand, the blue lines represent the surfaces that are modelled as thermal insulators and purple lines label distance parameters and are denoted as *d* or *x*.

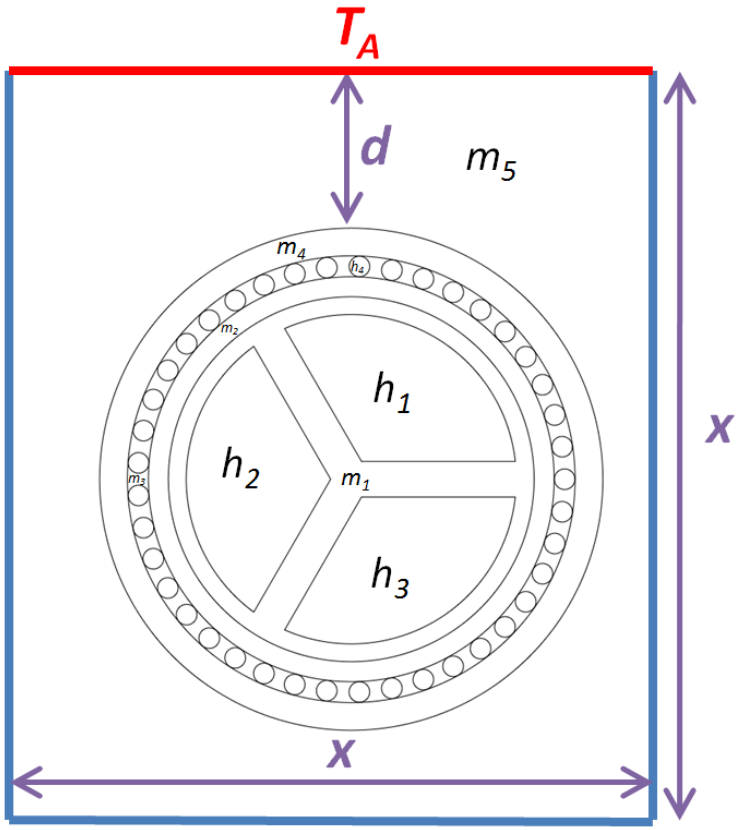

Figure 5: Cross sectional view of a 185 mm^2 Prysmian Waveform cable in a square box

The drawing is then imported into COMSOL and each of its objects is allocated the material properties of the component that they represent. In the particular case of the modelled LV waveform cable these material properties are provided in Table 3.

Table 3: The material properties used in the cable model

Error! eference source not found. **Label**	**Description** *185 mm^2 Prysmian Waveform cable*	Thermal Conductivity, k, $(\frac{W}{m \cdot K})$	Density, ρ, $\frac{kg}{m^3}$	Heat Capacity, C_p, $\frac{j}{kg \cdot K}$
m_1	XLPE	0.13	1300	900
m_2	Rubber bedding	0.15	1200	2000
m_3	Rubber bedding	0.15	1200	2000
m_4	PVC	0.19	1300	900
m_5	Soil	variable	variable	variable
h_1	Aluminium	204	2707	896
h_2	Aluminium	204	2707	896
h_3	Aluminium	204	2707	896
h_4	Aluminium	204	2707	896

Note that the material properties associated with soil are referred to as 'variable' in Table 3. This reflects the fact that the moisture content of the surrounding material is a factor that changes over time and one that is known to have an impact on thermal resistivity as noted in BS 7769. Also, thermal capacity changes in accordance with the moisture content of the surrounding medium. Therefore, the impact of the changing moisture content in the soil was investigated by observing thermal behaviour of the cable when the thermal resistivity and thermal capacity were varied so to replicate the impact of dry, regular and wet surrounding materials. The thermal conductivity for dry, regular and wet surrounding materials was taken from the IEC 60283 recommendations and 0.25 $\frac{\mathrm{W}}{\mathrm{m \cdot K}}$, 0.8333 $\frac{\mathrm{W}}{\mathrm{m \cdot K}}$, 1.4286 $\frac{\mathrm{W}}{\mathrm{m \cdot K}}$ were used respectively. Values for the thermal capacity of the soil were taken from a study that measured how it changed in sand when moisture was added and quantities of 720,000 $\frac{J}{kg \cdot K}$ 1,040,000 $\frac{J}{kg \cdot K}$ and 1,400,000 $\frac{J}{kg \cdot K}$ were used for dry, regular and wet surrounding mediums respectively.

A mesh is then defined in COMSOL which represents an interconnected network of individual nodes and the example for the LV waveform cable is shown in Figure 6.

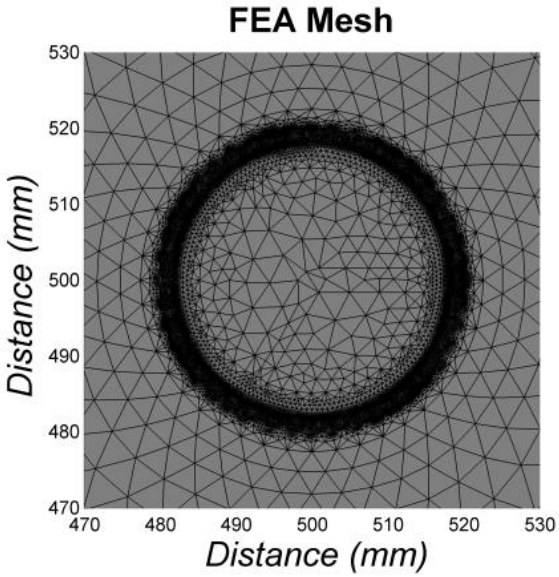

Figure 6: FEA Model Mesh of the LV Waveform Cable

The user executes simulations by specifying the simulation duration, simulation time step size and the inputs for all variables, such as phase current and ambient temperature, at every time step using MATLAB code which essentially runs the COMSOL model over the computer interface. COMSOL computes a solution for every node defined within its mesh at every simulation time step and MATLAB imports all of this data, which can be of very large size, for post-processing. Therefore, COMSOL acts as a single time-step FEA solver to MATLAB which handles the processing of all the inputs and outputs of the overall thermal model.

As indicated in the previous paragraph, FEA model computes temperature time-profile for each of the nodes. Therefore, the amount of data produced through evaluation of FEA model can easily become overwhelming and unmanageable. In order to address this issue the nodes are grouped into the layers. Then for each layer at every sampling instant both the maximum and the minimum temperature, found across all the nodes belonging to that particular layer, are identified and stored. In such a way the information from hundreds or even thousands of nodes can be compressed into a few variables, which makes handling of simulation data manageable. The layers associated with the cable are defined by forming concentric circles. Then the areas between adjacent concentric circles are designated as layers. Figure 7 shows the cross-sectional area of the LV waveform cable and the layers are numerically labelled from 1 to 5.

The innermost layer, labelled '1' in Figure 7, consists of the phase conductors and XLPE insulator. Therefore, this layer is termed Alu/XLPE layer. The second layer, labelled '2' in Figure 7, represents the concentric XLPE insulator and is termed XLPE layer. The third layer, labelled '3' in Figure 7, represents rubber bedding and is termed Rubber layer. The fourth layer, labelled '4' in Figure 7, contains neutral conductors as well as the surrounding rubber and is termed Rubber/Alu layer. The last layer of the cable itself, labelled '5' in Figure 7, is constructed of PVC. Finally, the sixth layer used in the FEA model designates the cable's surrounding medium which in the work reported in this report was assumed to be soil.

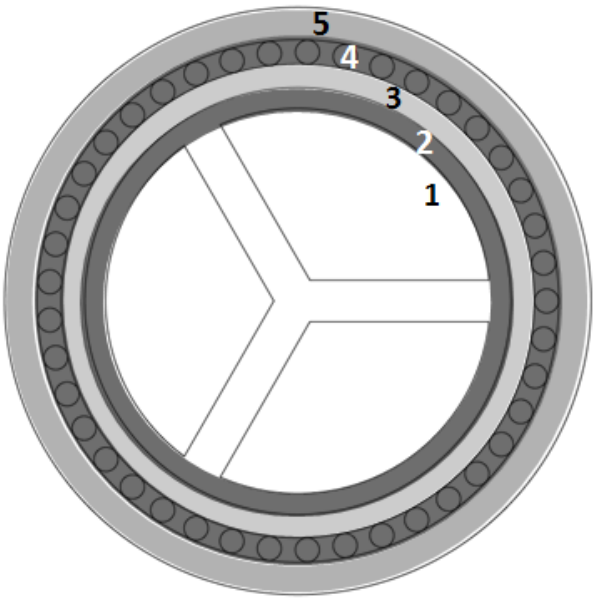

Figure 7: Layers of the LV waveform cable

As mentioned previously, all of the results shown in the subsequent sections of the report display either the maximum or minimum temperature reached across all the nodes in a particular layer.

Clearly, one could use other measures to represent the temperatures of all the nodes in a given layer at any point in time, such as the mean or median or mode. However, the key motivator for the work reported in this report was to avoid excessive temperature within the cable so the main concern was to identify the highest temperature within the cable. Therefore, the most frequently used measure to define cable temperature in this report will be maximum temperature in the layer that contains the main heat sources, i.e. Alu/XLPE layer.

2.2.3 Resolution of the FEA Mesh

The size of the FEA mesh, i.e. number of nodes used to describe a given system, impacts the accuracy of the numerical results that it produces but it also has a consequence on the computational effort required to carry out simulations. The FEA mesh of the thermal model developed for Prysmian Waveform cable was tested for its ability to capture data within each layer by running a simulation using a fine mesh and comparing the results to those obtained with a coarser mesh containing fewer nodes. The fine and coarse meshes, referred to as F-FEA and C-FEA, that were evaluated are shown in Figure 8.

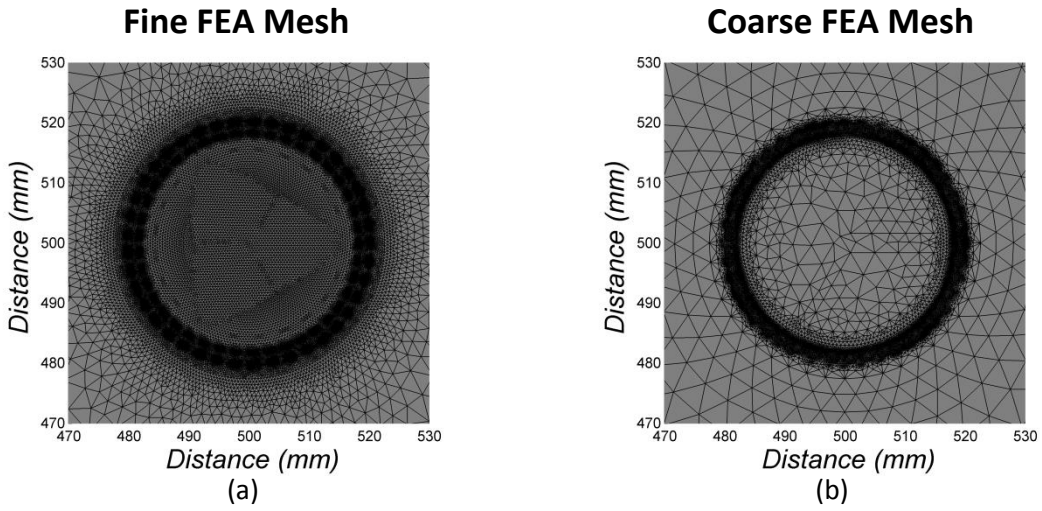

Figure 8: Graphical display of Fine FEA Mesh (a) and Coarse FEA Mesh (b)

The experiment was conducted by applying a step of 335A in each phase conductor whilst the ambient temperature was kept at 20°C. This step was applied to both the C-FEA model and F-FEA model and the maximum and minimum temperature for each layer were collected for both models. The difference between the temperatures obtained using the F-FEA and C-FEA is shown in Figure 9 for all the layers.

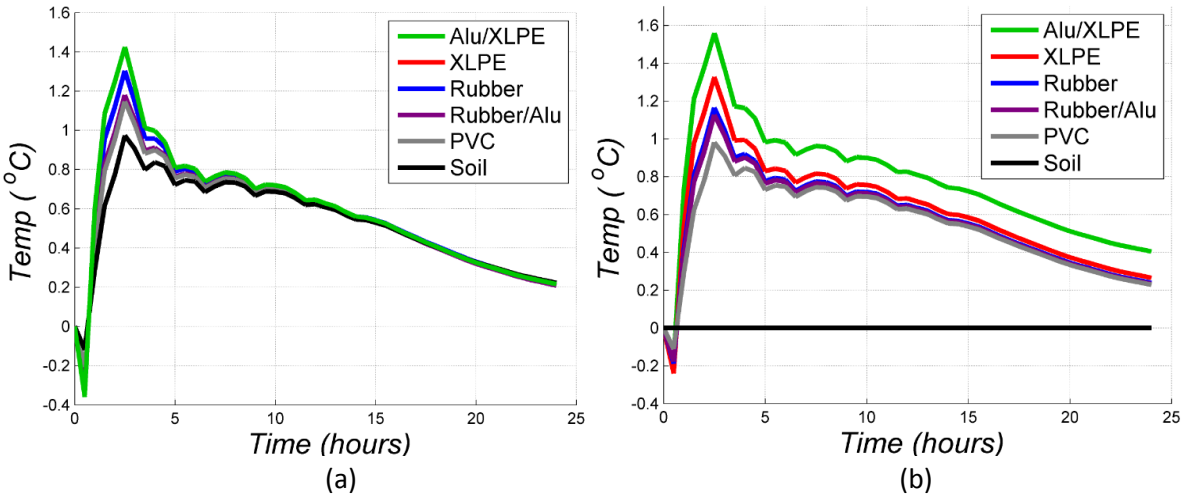

Figure 9: Difference in Maximum and Minimum Temperature for each of the layers between F-FEA Mesh and C-FEA Mesh

The largest temperature difference for both the maximum and minimum temperature occurs in the Alu/XLPE layer at approximately 2.5 hours and is approximately equal to 1.5 °C but it soon approaches zero as the temperatures converge to a steady-state. Comparison between the time profiles of maximum temperature in the Alu/XLPE layer obtained using C-FEA and F-FEA is shown in Figure 10.

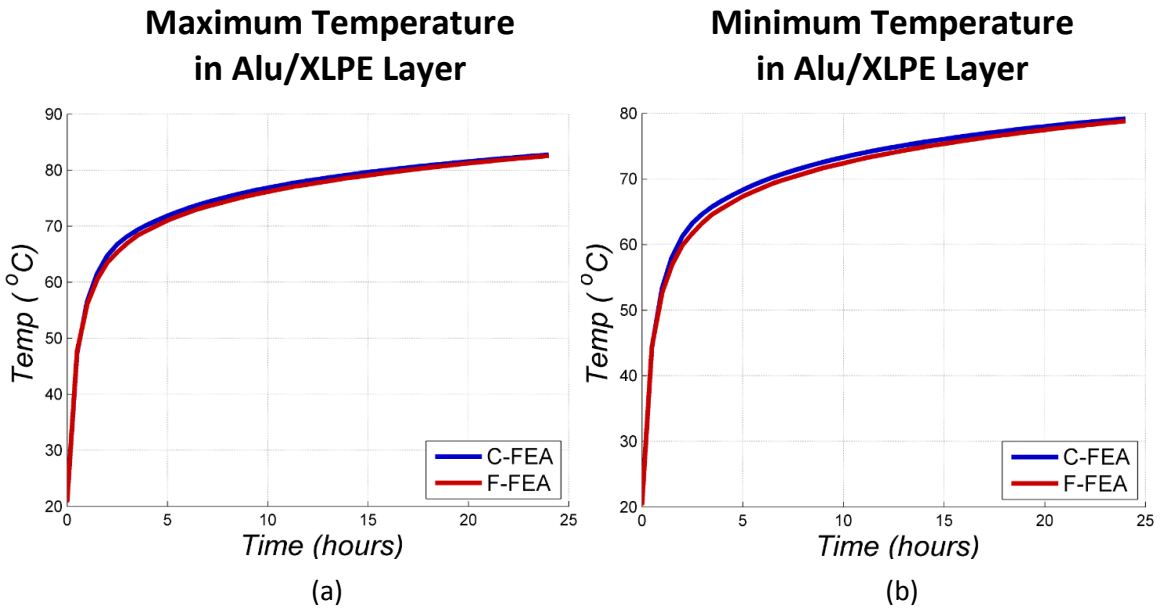

Figure 10: Comparison of C-FEA and F-FEA for Alu/XLPE layer

As can be observed from Figure 10, the difference is very small. Therefore, it was decided to proceed with the usage of the C-FEA model in order to minimise unnecessary computational burden whilst not significantly sacrificing the model accuracy.

2.2.4 Sizing of the Cable Surrounding Medium Area

The physical size of the cable's surrounding medium that is considered in the FEA model has a considerable impact on the computational speed. Also, in any future development of laboratory scale experiments concerned with thermal behaviour of a cable it will be critical to determine the physical size of the surrounding medium which itself will directly impact on the overall size of the experimental rig. Therefore, the objective is to optimise the size of the surrounding medium so that the results obtained are sufficiently close to the realistic case in which the cable's surrounding medium is unbounded in three directions but also for the size to be as small as possible in order to ensure adequate computational speed and/or feasible size of the experimental rig. The numerical experiment outlined in this section was used to determine the size of the surrounding medium that was then used in all the subsequent experiments.

Several FEA models were created that included 185 mm^2 Prysmian Waveform cable placed in the surrounding medium of variable size. A cross section of the models is provided in Figure 5. The parameter *d* denotes the burial depth of the cable and was kept to a constant value of 500 mm for all experiments. Also, the surrounding medium was assumed to be square shaped for each experiment with the length of each side, denoted as x in Figure 5, varied from 600mm to 2,000 mm.

The initial temperature of all the nodes in the FEA model was set to 20^{o}C and a constant phase current of 335A per phase conductor was applied for 24 hours. The maximum cable temperature was recorded at every minute and the resultant response is shown for different sizes of the surrounding medium in Figure 11.

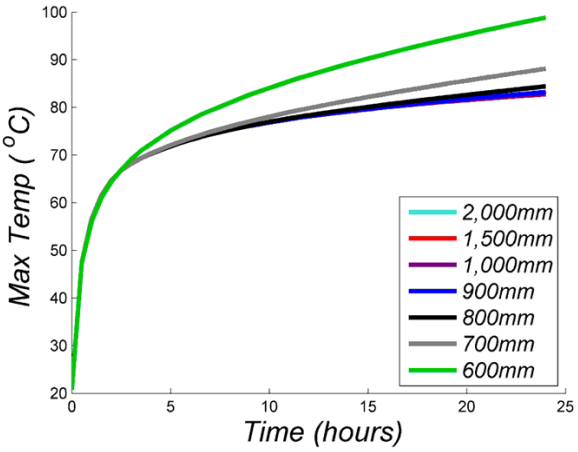

Figure 11: Cable temperature step responses for different sizes of surrounding medium

Temperature profiles shown in Figure 11 indicate that there is insignificant difference between the 1,500 mm and 2,000 mm step response results. Therefore, it was decided to set the parameter *x* to 1,500 mm. However, if considering scenarios that contain more than one cable or additional heat sources, the methodology used for this experiment would need to be repeated to validate the particular model as additional heat sources may require a larger area of surrounding medium.

3 Simulation Results

This chapter documents the results of experiments which were conducted to demonstrate the capability of the FEA thermal model and also to obtain some insight into the thermal behaviour of the underground LV cables. Pulse response experiments are firstly documented which provide a useful insight into thermal behaviour of the cable when the sudden changes in load occur. More specifically, they allow the user to better estimate the amplitude as well as duration of such sudden changes in load which would not violate the thermal constraint of the cable. Then the results related to modelling of the real LV network are documented that further demonstrate the capability of the thermal FEA model and show how it can be used to evaluate impact of various loads, such as electric vehicles, on the cable temperature.

3.1 Pulse Response Experiments

This section documents the results of the numerical experiments conducted using the FEA model of the LV waveform cable when subjected to sudden change in load that is maintained for a specific length of time. The key objective is to understand how quickly the cable temperature rises following a sudden step change in load.

As illustrated in Figure 12, applied current pulse and the resultant cable temperature response are characterised by 4 parameters, which are, the initial load (given as percentage of the rated cable current which is assumed to be equal to 335A per phase), amplitude of the pulse (given as a percentage of the rated phase current and denoted as $\Delta Load$), time duration of the pulse (which is denoted as t_{pulse}) and the final cable temperature that is reached at the end of a pulse (denoted as $T(t_{pulse})$).

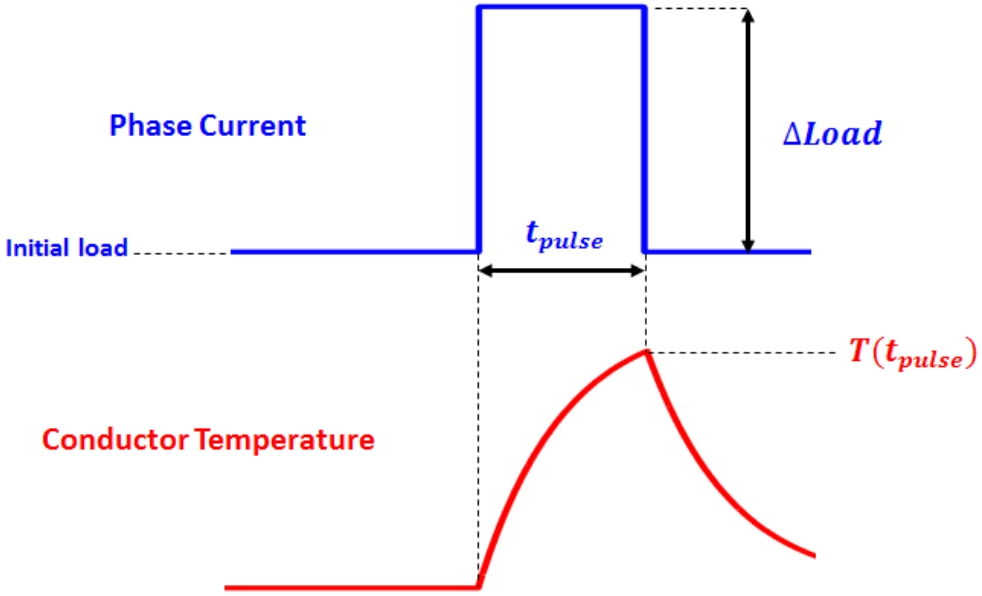

Figure 12: Illustration of Pulse Response

The initial experiment was conducted to demonstrate the impact that a balanced 335 A step change in phase currents has on the maximum and minimum temperatures experienced in each layer of LV waveform cable. For the experiment the simulation time was set to 24 hours, the thermal conductivity of the cable's surrounding medium was set to $0.833\frac{W}{m\cdot K}$, and the initial temperature of the cable, soil and ambient were set to 20°C. Hence, in the context of pulse response description shown in Figure 12, it was assumed for this experiment that $\Delta Load = 100\%$, $Initial\ Load = 0\%$, $t_{pulse} = 24\ hours$. The maximum and minimum temperature results for each of the six layers were collected for every sampling instant and are shown in the three dimensional plots of Figure 13.

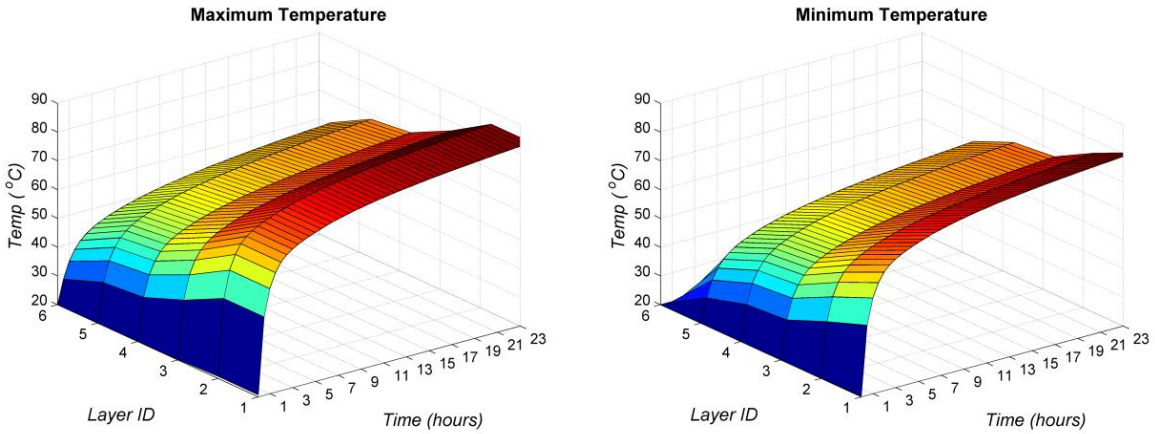

Figure 13: Maximum (a) and minimum (b) temperature response of the waveform cable to a balanced step change in phase currents; Layer ID: Alu/XLPE=1, XLPE=2, Rubber=3, Rubber/Alu=4, PVC=5, Soil=6

Simulation results shown in Figure 13 indicate a high level of cross-correlation between the temperatures of each of the six layers during the step response. This applies equally to both maximum and minimum temperatures within each layer. Also, it is clear that the rate of rise of temperature is more rapid in the layers that are located closer to the centre of the cable, which is somewhat expected since that is the location of the main heat sources, i.e. phase conductors. Finally, it can be observed that the first two layers (Alu/XLPE and XLPE) are consistently and visibly hotter at any point in time when compared to Rubber layer and other layers located further away from the cable's core.

All the subsequent pulse response experiments were conducted by varying initial load and amplitude as well as duration of the applied pulses of phase current. Furthermore, experiments were conducted for two different ambient temperature values to reflect seasonal changes and also for three different levels of soil moisture.

Initial load values used in the experiments were 10%, 25%, 50% and 100% of the rated cable current. Amplitude of the pulse was equal to either 25%, 50% or 100% of the rated cable current. Ambient temperature was set to be equal to either 8^{o}C when assuming the winter season or 17^{o}C when assuming the summer season. Finally, three different levels of soil moisture content were designated as 'dry', 'regular' and 'wet'. Their corresponding values of soil's thermal resistance and capacity are described in Section 2.2.2 on page 13. Therefore, 72 experiments in total were conducted. Results from all 72 experiments are provided in tabular form in Appendix A1.

In order to appropriately initialise the thermal model prior to the application of the step change in load the simulations were firstly run for 90 days with constant initial load and constant ambient temperature. Whilst it may be considered unrealistic that the cable current is kept constant at a certain level for 90 days such a scenario can be thought of as equivalent to that of having an average load equal to that same certain level for some time prior to the step change in the load. This equivalence is justified by the argument that the presence of thermal inertia would inevitably filter out short-term load variations as well as ambient temperature variations.

Examples of resultant pulse responses are shown in Figure 14 for two different amplitudes of load step change. In both cases summer season and the dry soil moisture content are assumed. Trends shown are those of maximum temperature associated with Alu/XLPE layer, Rubber/Alu layer and PVC layer.

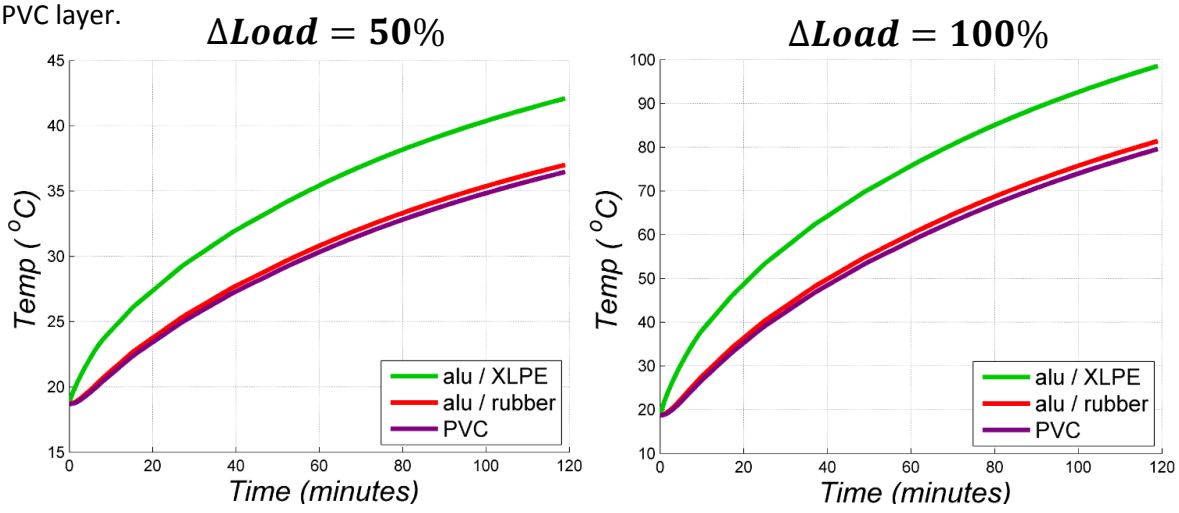

Figure 14: Plot of pulse responses of cable temperatures during summer season and with initial load of 10%

Note that thermal resistance in the cable layers creates continual difference between temperatures in these three layers at any point in time. However, since Rubber/Alu and PVC are adjacent layers, the difference in temperature is not as pronounced as in the case of Alu/XLPE layer. In both cases the initial load is the same and equal to 10% but the step change of load is different and therefore the speed at which the temperature reaches a certain threshold will also be considerably different. In particular, Figure 14(a) shows that when the step change in load is equal to 50% of the rated cable current then the maximum temperature inside the Alu/XLPE layer reaches 40 °C after approximately 100 minutes. On the other hand, in the case of a step change equal to 100% of the rated cable current the maximum temperature inside the Alu/XLPE layer reaches the same threshold of 40°C in just 10 minutes as shown in Figure 14(b).

In order to explore the dependence of the cable temperature on the initial load as well as the soil moisture content for various amplitudes and durations of the pulse, additional graphs were generated which express cable temperature reached after certain length of time as a function of initial load. In total, 30 of these figures were generated and are provided in Appendix A2. In this section three examples of these graphs are shown in Figure 15 to demonstrate interpretation of the results displayed. These figures allow an engineer to quickly and relatively easily determine the temperature reached inside a cable for a given value of the initial load, for the given amplitude and duration of the load pulse as well as for different soil moisture content.

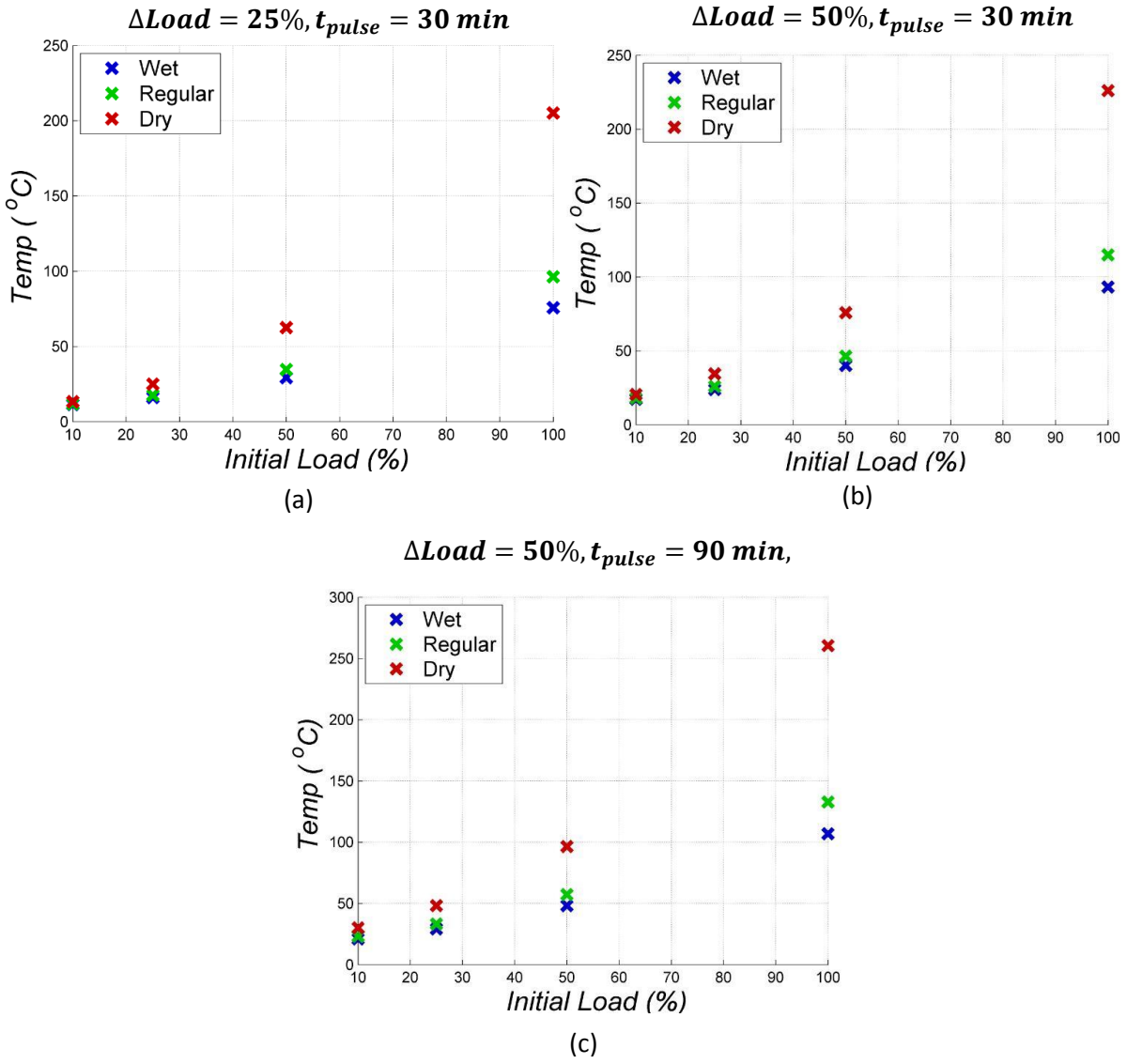

Figure 15: Scatter plot of cable temperature for different values of initial load and soil moisture content

The first clear observation from all the plots shown in Figure 15 is the parabolic relationship between the initial load and the cable temperature reached at the end of a pulse for any of the three soil

moisture content levels. Such a relationship is expected since the phase current is related to heating power through the quadratic/parabolic relationship. Figure 15(a) shows the temperature reached 30 minutes after the step change of 25% is applied and assuming winter season. It can be observed from this figure that the temperature will remain less than 100^{o}C for any value of initial load provided the moisture content of the soil is classed as either regular or wet. Also, if the dry soil condition is assumed then the temperature will rise beyond 80^{o}C for any initial load greater than approximately 50%. If the step change in load is increased to 50% and the resultant pulse lasts for 30 minutes then, as shown in Figure 15(b), the resultant cable temperature will exceed 100^{o}C for regular soil moisture content and for initial load of 100%. If the time duration of the pulse is extended to 90 minutes then, as shown in Figure 15(c), the cable temperature will exceed 100^{o}C for any soil moisture content and for initial load equal to 100%. Also, the maximum cable temperature reached when a pulse of 90 minute duration is applied will reach 100^{o}C assuming dry soil conditions even for an initial load equal to 50%.

The final observation is a clear divergence in cable temperature caused by different soil moisture content and its high level of dependence on the magnitude of the initial load, as is evidently observed in all graphs in Figure 15. This dependence arises because initial load has a direct and dominant impact on the initial cable temperature, which in turn has an obvious impact on the temperature reached after a given pulse of load current is applied.

Next the pulse response trends of maximum cable current are shown in the time-domain in Figure 16 but with two traces displayed on each of the plots. The blue trace represents the best-case scenario which corresponds to winter season with wet soil condition. The red trace represents the worst-case scenario which corresponds to summer season with dry soil condition. In total, 12 of these plots are provided in Appendix A3 and here the focus is on 4 particular graphs shown in Figure 16.

Firstly, Figure 16(a) shows the pulse responses resulting from the step change in load equal to $\Delta Load = 100\%$ with the initial load equal to 10%. In this particular case, it is observed that in the worst-case scenario the thermal constraint, assumed to equal 80 ^{o}C, is reached approximately 70 minutes after the step change is applied. On the other hand, in the best-case scenario thermal constraint is not going to be violated for a pulse of any time duration. Next, in Figure 16(b) the initial load is increased to 25% and it is noticed that the time it takes for the cable temperature to reach the thermal constraint is reduced to 35 minutes in the worst-case scenario. On the other hand, in the best-case scenario thermal constraint is reached only if the step change in load is kept for a very long time, i.e. many hours. However, by increasing the initial load to 50% it is observed in Figure

16(c) that the time it takes to reach thermal constraint is reduced significantly in both worst-case and best-case scenarios. In the worst-case scenario it now takes 5 minutes to reach 80°C whereas in the best-case scenario it takes 40 minutes for the cable temperature to reach 80°C. Finally, Figure 16(d) shows the result of maintaining the initial load at 50% but reducing the size of the load change from $\Delta Load = 100\%$ to $\Delta Load = 50\%$. Then in the best-case scenario the thermal constraint is not reached regardless of how long the pulse of current is maintained for. Also, in the worst-case scenario the time to reach thermal constraint is increased from 5 minutes to 20 minutes.

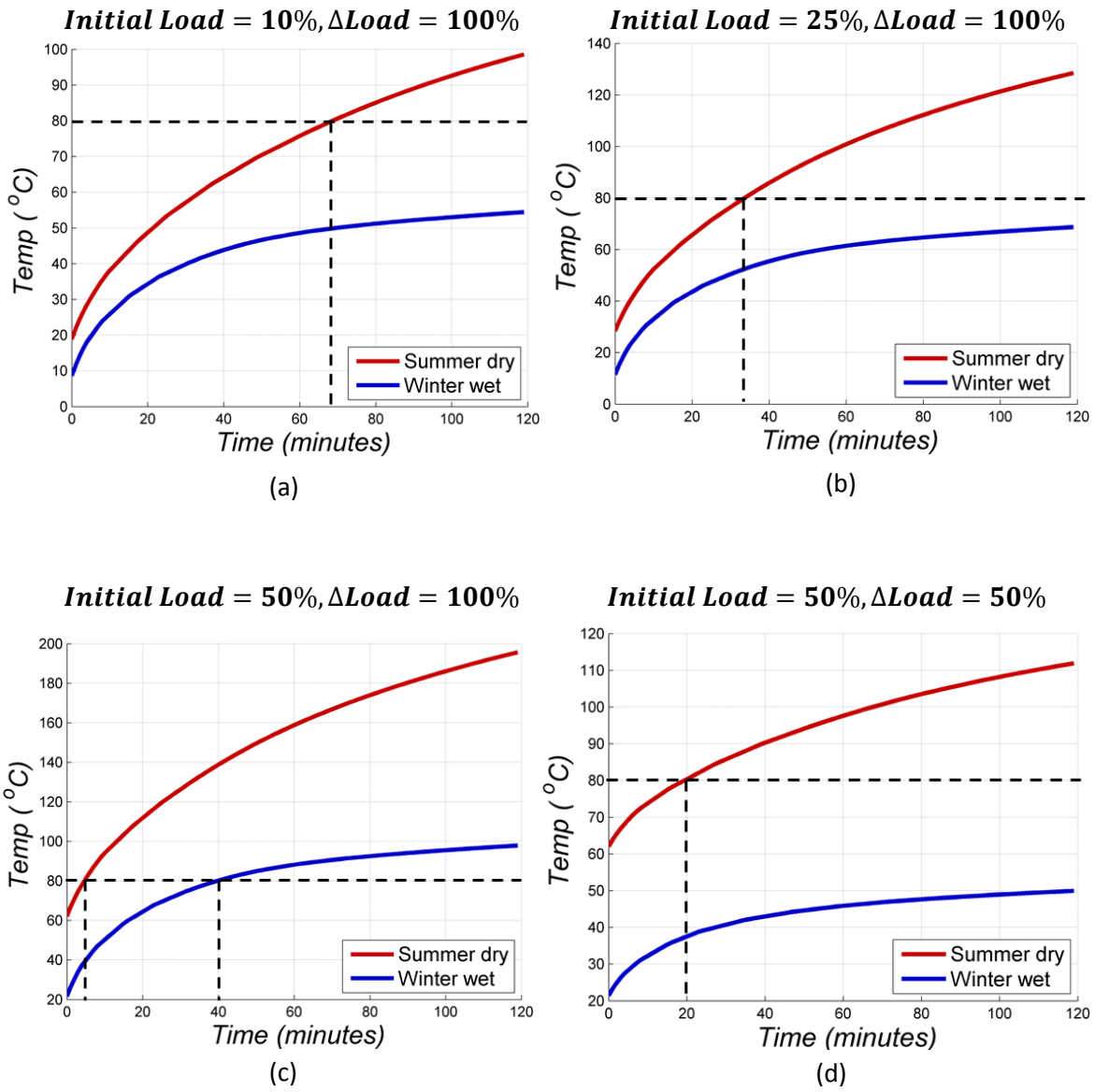

Figure 16: Pulse response of cable temperature for summer season dry soil condition, i.e. the worst case, and for winter season wet soil condition, i.e. the best case

An additional important observation, already briefly mentioned earlier in this section, and particularly evident in Figure 16(d) concerns visible discrepancy in the initial temperature between

the best-case and worst-case scenario. In particular, initial temperature of the worst-case scenario is 40°C higher than the initial temperature of the best-case when the initial load is equal to 50%. This is contrasted to the difference of just 10°C shown in Figure 16(a) in which initial load is reduced to 10%. This confirms the observations based on results shown in Figure 15 that the initial load has a significant impact on the temperature reached after the pulse has been applied through its impact on the initial temperature.

Overall, the most striking observation from the pulse response experiments is the impact that the soil moisture content has on the thermal behaviour of the cable both in terms of the steady state and dynamic response. As a result of its steady-state impact, the initial temperature prior to the application of the pulse is strongly influenced by the soil moisture content. Then, once the pulse is applied, the difference in response is increased even further. On the other hand, differences in seasonal ambient temperature appear to make directly proportional rather than amplified impact on the cable temperature response. In other words, seasonal variation in ambient temperature is replicated in cable temperature.

3.2 Dynamic Thermal Modelling of a LV Network

Developed thermal models can be readily integrated with the electrical models of a given distribution network in order to assess the impact of various novel low-carbon technologies, such as electric vehicles and photovoltaic panels, as well as traditional loads on a distributor's cable temperature over time. For this purpose, an example experiment was devised which focuses on the impact of electric vehicles and is detailed in this section. This experiment can also be adapted to assess the thermal impact of incorporating other low-carbon technologies and/or demand side management schemes. Firstly an electrical model is used to determine realistic phase current profiles and then these phase currents are used as inputs to the thermal model in order to calculate temporal variation of temperature in the distributor's cable.

3.2.1 Development of the Electrical Model

The distributor used to demonstrate the capability of the thermal models is part of ENW's low voltage distribution network and is shown in the single-line diagram provided below where arrows indicate a dwelling load, circles indicate a street lamp and numbers denote particular phase connections.

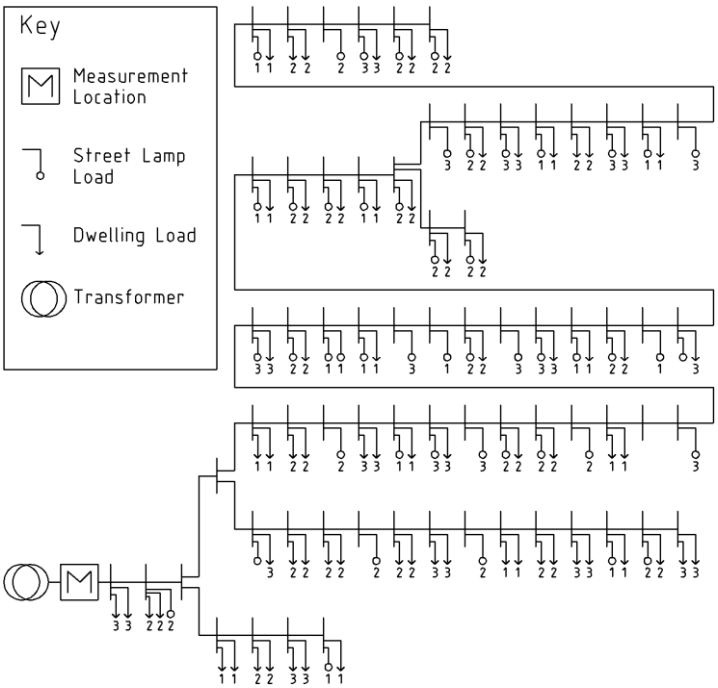

Figure 17: Example distributor network

OpenDSS [7], which is a comprehensive electrical power system simulation tool, was used to model the electrical behaviour of this distributor and its loads. The reason for the usage of OpenDSS is its straightforward interface to MATLAB software package which enables a seamless data link between electrical model and the FEA thermal model. The network was first modelled without any EVs which enabled the model to be validated by comparing data that it generated with real data from the DNO trial [8]. The real data consists of five minute mean r.m.s phase and neutral conductor currents which were measured at the location highlighted as the "Measurement Location" that is adjacent to the 11kV/415V secondary transformer. This particular "Measurement Location" was also assumed to be a 'hot spot' which would experience highest current and, therefore, the highest temperature in the distributor. Each of the loads shown in Figure 17 was configured as a constant power load with a pf of 0.97 to match the measured local aggregate reported in [8]. Unique load profiles were generated using the CREST 'high-resolution energy demand model' [9] for each of the dwellings which were then used as inputs to a power flow simulation. Two example load profiles which were generated from the CREST model are provided as a reference in Figure 18.

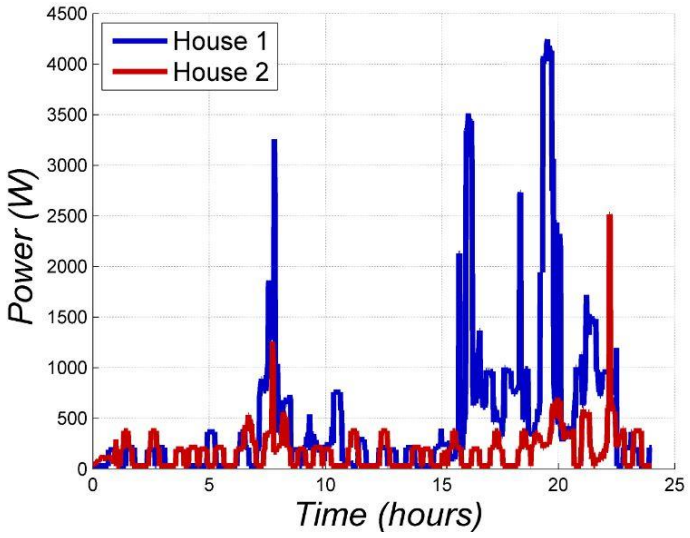

Figure 18: Two examples of single dwelling load profiles created using the CREST model

The example feeder was surveyed using Google street view where it was found to consist of two, three, four bedroom houses as well as one and two bedroom flats. The most common type of dwelling connected to the distributor was observed to be the two bedroom house, and as data on the occupancy level of each dwelling was not available, it was assumed that each dwelling was occupied by three people.

In OpenDSS, the resistance ***R***, inductive reactance ***X*** and capacitance ***C*** matrices were used to specify the electrical cable parameters and were constructed as follows:

$$\boldsymbol{R}=\begin{bmatrix} R_s & R_m & R_m & R_m \\ R_m & R_s & R_m & R_m \\ R_m & R_m & R_s & R_m \\ R_m & R_m & R_m & R_s \end{bmatrix}, \boldsymbol{X}=\begin{bmatrix} X_s & X_m & X_m & X_m \\ X_m & X_s & X_m & X_m \\ X_m & X_m & X_s & X_m \\ X_m & X_m & X_m & X_s \end{bmatrix}, \boldsymbol{C}=\begin{bmatrix} C_g & C_c & C_c & C_c \\ C_c & C_g & C_c & C_c \\ C_c & C_c & C_g & C_c \\ C_c & C_c & C_c & C_g \end{bmatrix} \quad (3)$$

DNO sequence component data was used to find the matrix elements above by applying the equation outlined below which is justified when cable lengths are short [10].

$$R_s=\frac{(2R_1+R_0)}{3},\ R_m=\frac{(R_0-R_1)}{3},\ X_s=\frac{(2X_1+X_0)}{3},\ X_m=\frac{(X_0-X_1)}{3} \quad (4)$$

In Eq(4) the subscripts *s* and *m* denote the self and mutual positive sequence components whilst the subscript 0 denotes zero sequence component. Conductor to conductor capacitance C_s was modelled by equating it to the positive sequence component whilst conductor to ground capacitance was assumed to be negligible and set to zero.

Most cables detailed in the DNO data obtained for the example distributor have four conductors but of those that had three, the specific electrical properties of the neutral conductor were not included. Therefore, all cables were modelled with the assumption that the phase and neutral conductors have identical electrical properties.

The real network data from the DNO trial [8] was measured on Thursday 1st November 2012. This data consists of the 5-minute mean rms measurements of phase voltages and phase and neutral currents shown in Figure 19.

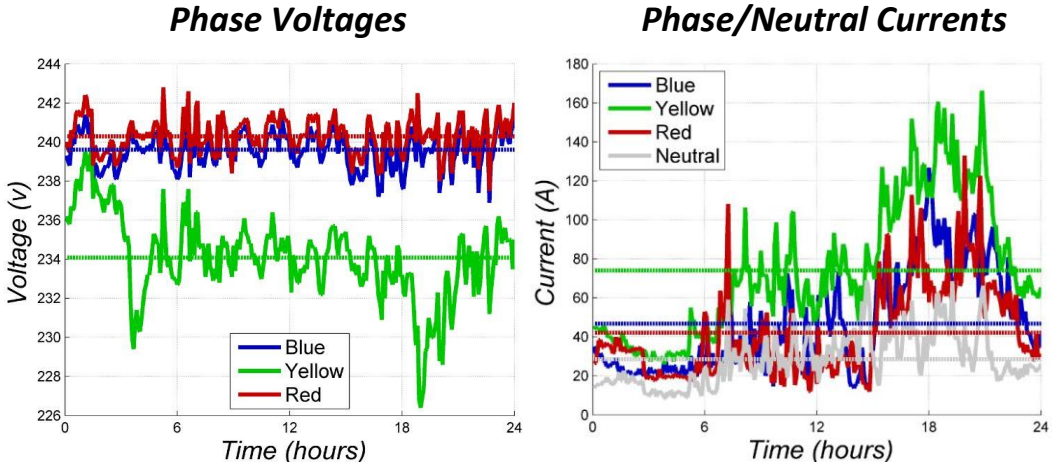

(a) (b)

Figure 19: Measured phase voltages (a) and phase and neutral currents (b) collected from the real distribution network at the 'Measurement Location' in Figure 17

Validation was performed by comparing the phase and neutral current trends collected from the real network with the current trends that the OpenDSS model generated when the real measured voltage data shown above and load profiles from the CREST model for a weekday in November were used as inputs. The implied underlying assumption in using the real voltage data is that its unbalance is inherited entirely from the other feeders connected to the same secondary winding of the transformer.

The phase and neutral currents obtained from the real network and the currents computed using the OpenDSS-based electrical model are compared in Figure 20.

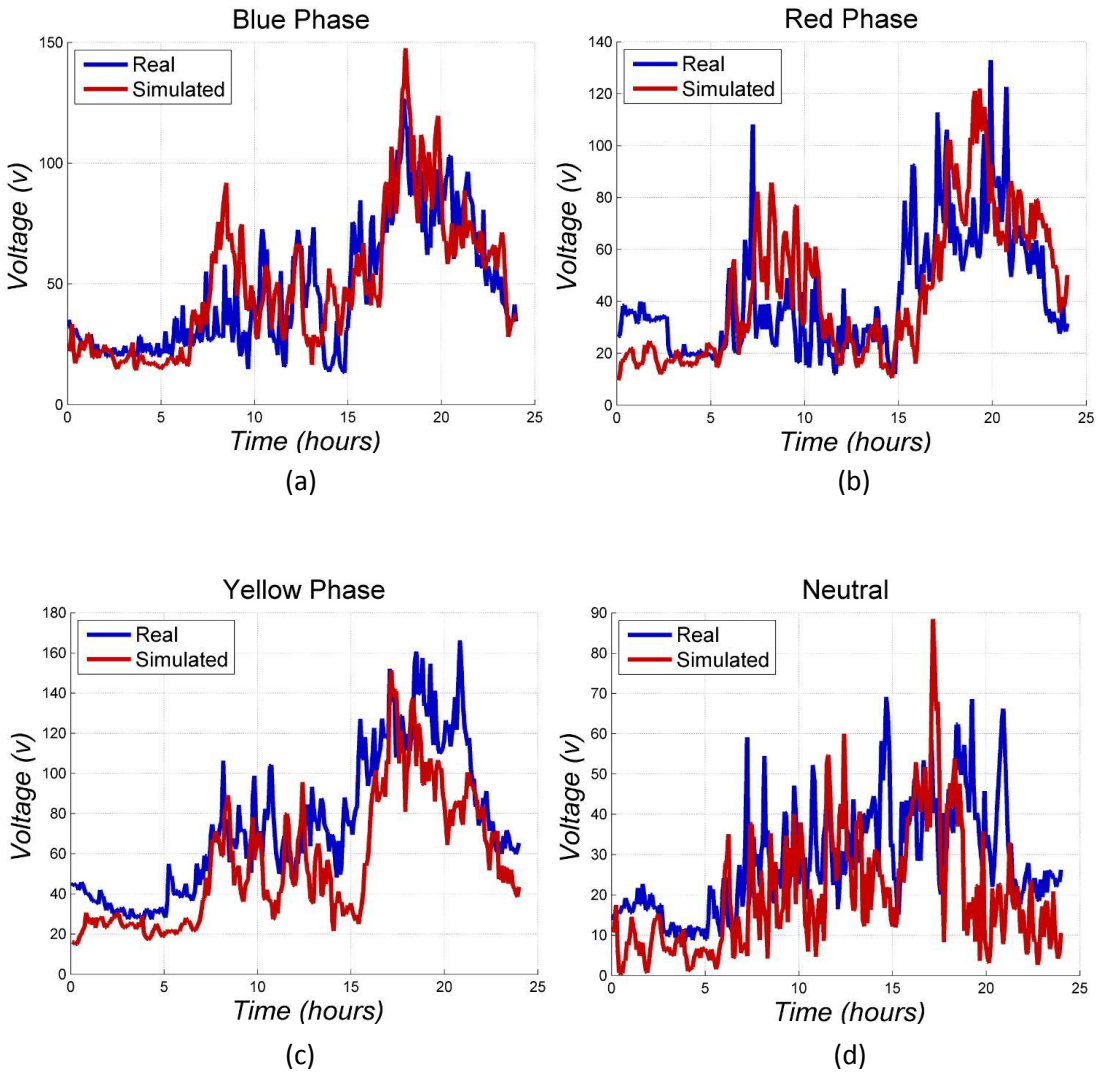

Figure 20: Phase and neutral current trends of the real distribution network (red) and the equivalent simulated distribution network (blue)

Visual inspection of these trends indicates sufficient level of similarity between the currents obtained from the real network and those obtained using the OpenDSS model.

In order to allow a fair comparison with the manufacturer's rating of this cable, it was assumed that the equal number of dwellings is allocated to each of the phases. This was done because balanced phase currents are assumed in cable rating calculations. Before any EVs were allocated to dwellings, a simulation was run to find the phase currents in the cable corresponding to EV penetration of 0% and the resultant phase currents are shown in Figure 21.

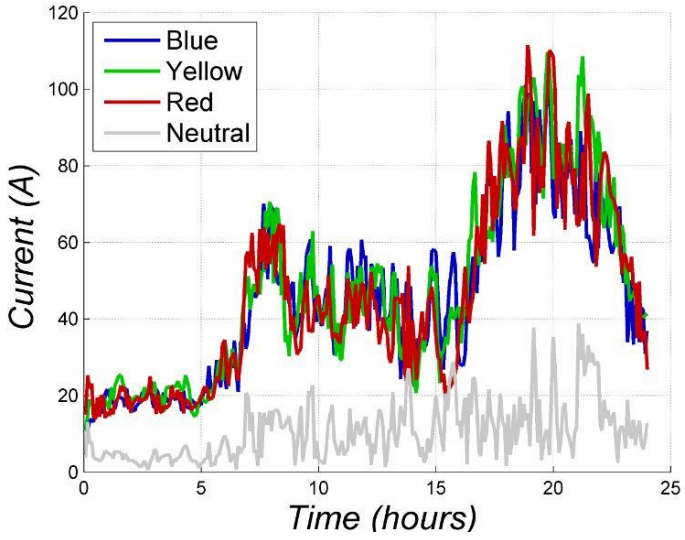

Figure 21: Cable phase currents generated by the OpenDSS model at the 'Measurment Location' highlighted in Figure 17

3.2.2 Evaluation of the Thermal Model

The next step was to apply the resultant phase and neutral currents obtained using OpenDSS to the thermal FEA model of the distributor's cable in order to determine the corresponding temperatures during the 24 hour period. As mentioned previously, the particular cable that was assumed to experience the highest current and therefore the highest temperature, i.e the hot spot, is located at the "Measurement Point" shown in Figure 17, and that cable was modelled using the thermal FEA model as a 185 mm^2 Prysmian waveform cable. The thermal conductivity of the cable's surrounding medium was set to 0.8333 $\frac{W}{m \cdot K}$ and the initial temperature in all the layers was set to 20^{o}C. Initially the simulation was run in the absence of any EV allocated to dwellings in order to establish the baseline performance in terms of the cable temperature. The maximum and minimum temperature values were collected for every layer and sampling instant and they are presented in three dimensional forms in Figure 22.

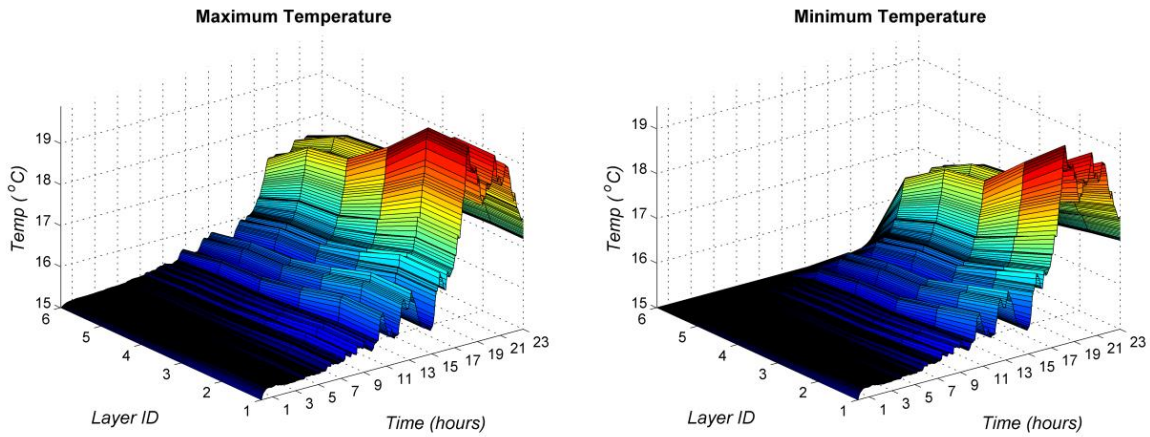

Figure 22: Three-dimensional display of maximum and minimum layer temperatures in the simulated distribution network cable during 24 hour period; Layer ID: Alu/XLPE=1, XLPE=2, Rubber=3, Rubber/Alu=4, PVC=5, Soil=6

As expected there is a significant cross-correlation in temperature across the layers as time progresses. As the cable loading increases or decreases so do the temperatures in all the layers. Also, layers located further away from the centre of the cable consistently experience lower temperature at any point in time, which is somewhat expected since the main heat source is located in the first layer. Finally, the first two layers (Alu/XLPE and XLPE) are observed to have very similar maximum temperature profiles throughout the simulation whereas the difference between their respective minimum temperatures tend to be more pronounced. Very similar observations were also made for the step response behaviour of cable temperatures in each of the layers in Section 3.1.

Once the thermal model was evaluated in the absence of any EV connections the next step was to consider the scenarios of varying EV penetration in the studied LV network. EVs were incorporated into the electrical model of the network by representing each of them as 3.8kW constant power sink.

Five further simulations were then run with varying levels of EV penetration. For each of the five simulations it was ensured that an equal number of EVs was allocated to each phase in order to maintain phase current balance and enable a fair comparison with the manufacturer's cable rating. The EVs were assumed to have a synchronised charging interval between 18:30 and 21:00 hours, which when applied to the OpenDSS model resulted in the phase current traces shown in Figure 23.

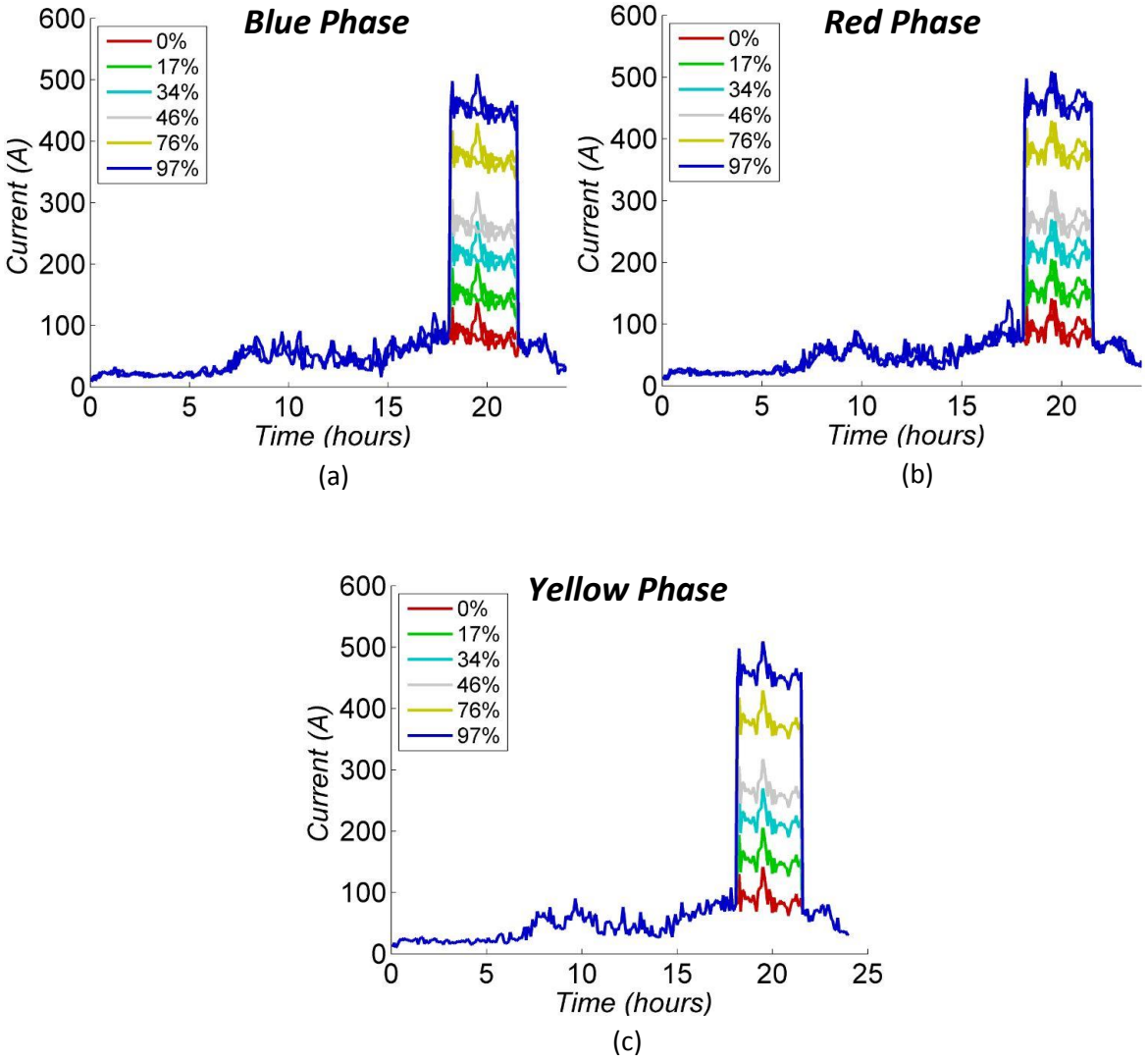

Figure 23: Phase currents for different levels of EV penetration in the simulated distribution network

A sudden change in each of the phase currents at 18:30 and lasting until 21:00 is a direct result of connecting EVs to their charging points.

The corresponding heating power traces, obtained by squaring phase currents and then multiplying them by the individual phase resistances of the waveform cable, are shown in Figure 24. Notice how, due to the squaring of the current in order to obtain the heating power, the sudden change in the cable loading that results from the penetration of EVs is much more prominently shown in Figure 24 when compared to Figure 23.

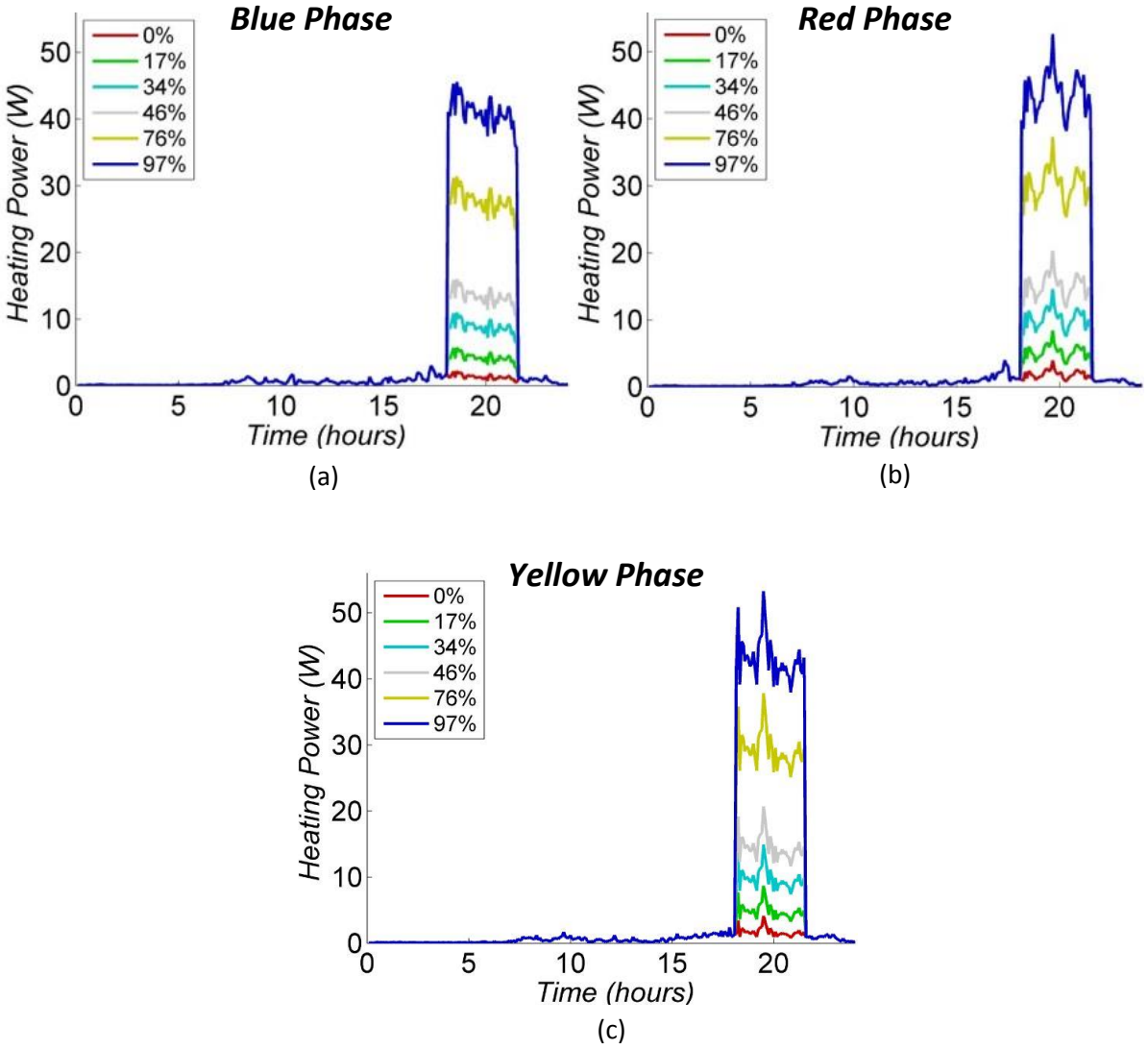

Figure 24: Phase conductor heating powers for different levels of EV penetration in the simulated distribution network

For each of the six EV penetration levels the simulation time was set to 24 hours, the sampling rate used was 1 min, the thermal conductivity of the cable's surrounding medium was set to 0.8333 $\frac{W}{m \cdot K}$ and the ambient ground temperature was set to 20°C. In each of the six experiments, the maximum temperature in the aluminium / XLPE layer was collected and is plotted in Figure 25.

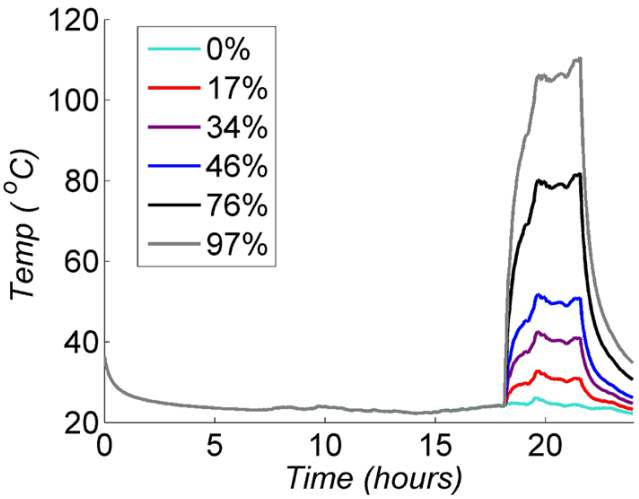

Figure 25: Maximum temperatures of the aluminium / XLPE layer of a waveform cable for different levels of EV penetration in the simulated distribution network

This result suggests that if 80°C is the cable's thermal constraint, which was quoted by the manufacturer in their rating calculation, the EV penetration capacity for this cable is approximately equal to 76% of the dwellings, assuming equal distribution of EVs across the three phases.

In order to maximise the allowed penetration of EVs whilst satisfying the thermal constraint the possible charging schedule taking form of a synchronised duty ratio across all EVs located on a given network segment could be deployed. Such a modified charging schedule would utilise the presence of thermal inertia in order to allow overloading of the cable during short-term bursts and then allowing it to cool down during the off-period. By modifying the charging duty cycle of the electric vehicles the maximum temperature reached by the cable can be directly affected. Figure 26 shows the temperature variation assuming the duty cycle is 50%. This figure shows that by introducing a synchronised duty ratio as a charging schedule strategy of demand side management the level of EV penetration can be increased to virtually 100% without violating thermal constraint. Clearly, by reducing the duty cycle the overall charging time is increased but the maximum temperature reached by the cable is reduced. Conversely, by increasing the duty cycle above 50% (i.e. period of charging is greater than the idle period of not charging) the maximum temperature does increase although the total time it takes to charge the vehicle is reduced.

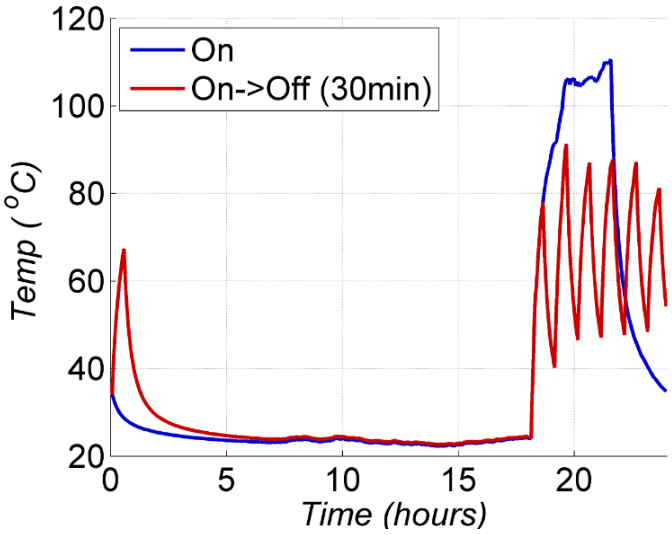

Figure 26: Maximum temperatures of the aluminium / XLPE layer of a waveform cable for different charging strategies and with 97% of EV penetration in the simulated distribution network

Whilst the results provided in this section assume a perfectly balanced network, in order to maintain a fair comparison with the manufacturers' ratings such assumptions can be readily removed and the thermal behaviour of unbalanced distribution networks can be obtained, which is expected to cause further increase in cable temperature. This is because in addition to phase currents supplying the loads on a network and representing a major source of heat, neutral current would also contribute to temperature rise.

Finally, it is important to note that other low-carbon technology loads, e.g. heat pumps, and distributed generation devices, e.g. PV, could also be incorporated into the distribution network model in order to assess their impact on the thermal behaviour of the underground cables.

4 Development of the Simplified Thermal Modelling Tool

Using the simulation results from the pulse response experiments, which are documented in section 3.1, a simple-to-use low-voltage cable thermal modelling tool, referred to here as LV-TM, was developed. LV-TM is based on the interpolation of the pulse response results, detailed in Appendix A1, which was performed in order to derive relatively simple algebraic expressions relating ambient temperature, initial load and step change in load to the maximum temperature reached inside the Alu/XLPE layer at specific time increments, after the step change in the load is applied. These identified algebraic relationships are provided in the Appendix A4.

The current version of LV-TM considers a particular type of cable current profile, which is a constant amplitude step/pulse preceded by constant initial current, and it assumes user-specified constant ambient temperature. In its current form LV-TM tool computes estimates of cable temperature for each of the three specific soil moisture contents levels, which are 'dry', 'regular' and 'wet' as defined in section 2.2.2, rather than an arbitrary user-specified moisture content level. Nevertheless, LV-TM provides a useful initial version of an easy-to-use thermal modelling tool, which is implemented in Microsoft Excel, that allows an engineer to evaluate the impact of various step/pulse changes in the cable loading and the impact they have on the cable temperature.

Also, the methodology that is used to develop this tool can be extended to other cable types and/or feeder arrangements in the future. Additionally, LV-TM can be extended to other time-varying load and ambient temperature profiles as well as different types of soil and levels of soil moisture content.

The following inputs are specified by the user in the current version of the LV-TM tool:

- Initial load, expressed as percentage of the assumed rated cable current, which is 335A per phase.
- Step change in load, expressed as percentage of the assumed rated cable current, which is 335A per phase.
- Ambient temperature in expressed in ^{o}C and assumed to be constant.

Once these values are entered, LV-TM computes an estimate of the maximum temperature inside the Alu/XLPE layer of the LV waveform cable at discrete 15-minute increment time steps proceeding step change in load and up to 120 minutes after the step change is applied. These cable temperature estimates are provided in tabular form within LV-TM tool for each of the three soil moisture content levels. Finally, the user is provided with the plot of the resulting three cable temperature responses, one for each soil moisture level.

A screenshot of the current version of the LV-TM tool is provided in Figure 27.

Low Voltage Underground Cable Thermal Modelling Tool

Initial Load (%)	25
Step Change in Load (%)	80
Ambient Temperature (degC)	17

Cable Temperature (Alu/XLPE Layer)			
Time	Dry	Wet	Regular
0 min	28.3	20.4	21.6
15 min	47.8	38.2	39.9
30 min	59.9	46.8	48.9
45 min	68.0	50.7	54.6
60 min	75.4	53.1	59.2
75 min	81.9	55.5	62.1
90 min	87.4	56.8	64.3
105 min	92.6	58.4	66.1
120 min	96.7	59.5	68.0

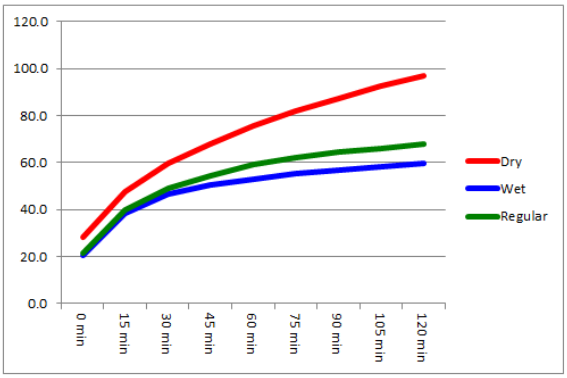

Figure 27: Graphical User interface of the LV-TM Tool

5 Conclusions

This report details the development of a dynamic thermal model of the low-voltage waveform cable that relates current passing through the cable to the cable temperature.

The cable considered in this study was Prysmian Waveform cable that was modelled using a high-fidelity Finite Element Analysis approach. The resultant model was subjected to a number of numerical experiments in order to better understand the dynamic thermal behaviour of the underground cable and the impact of various environmental factors such as moisture content in the soil and seasonal changes in ambient temperature.

Simulation results demonstrated ability of the LV waveform cable to sustain short-term pulses of high-amplitude phase currents without exceeding the thermal constraint. In addition, the key observation from these numerous simulations was that the moisture in the soil had a significant impact on the thermal behaviour of the cable. In particular, dry soil conditions significantly increased the temperature experienced inside the cable and therefore reduced the current carrying capacity of the cable. On the other hand, wet soil conditions lowered the temperature and allowed high levels of increased current to flow through the cable without violating thermal constraint. Whilst soil moisture content had a significant impact on the cable temperature, the impact of seasonal changes on ambient temperature had a much smaller, linear and directly proportional impact on the cable temperature. In fact, average ambient temperature difference between seasons was replicated in the seasonal temperature difference inside the cable.

Developed model was also used to show how the impact of incorporating low-carbon technologies on the thermal behaviour of the cables can be assessed in order to inform future network design as well as future operational considerations, such as demand side management (DSM). It was shown how the modification of a charging schedule of electric vehicles that introduces a synchronised duty cycle can allow significant increase in their penetration level whilst satisfying thermal constraint.

Simplified dynamic thermal model of the LV waveform cable was derived and implemented using Microsoft Excel. This simplified model allows user to specify initial cable loading and the step change in the cable current as well as the ambient temperature in order to observe cable temperature time-profiles for three different soil moisture content levels.

6 Bibliography

[1] K. Qian, C. Zhou, M. Allan, and Y. Yuan, 'Modeling of Load Demand Due to EV Battery Charging in Distribution Systems', *IEEE Transactions on Power Systems*, vol. 26, no. 2, pp. 802–810, May 2011.

[2] British/ International Electrotechnical Commission, 'Electric cables — Calculation of the current rating. BS IEC 60287'. BS IEC, 2007.

[3] S. British, 'LV and MV polymeric insulated cables for use by distribution and generation utilities'. BS 7870, 2011.

[4] Energy Networks Association, Engineering Recommendation P17 - Current Ratings for Distribution Cables, 1976.

[5] D. Miller, D. Yellen, D. Hollingworth, 'A Review of Engineering Recommendations P15, P17 and P27 (Transformers, Cables and Overhead Lines)', [Online]. Available: http://www.networkrevolution.co.uk/project-library/review-engineering-recommendations-p15-p17-p27-transformers-cables-overhead-lines/, [Accessed: 29-Jun-2015].

[6] P. Davison, 'Real-Time Thermal Rating – Underground Cables', [Online]. Available: http://www.networkrevolution.co.uk/project-library/clnr-trial-analysis-real-time-thermal-rating-underground-cables-2/, [Accessed: 29-Jun-2015].

[7] Electric Power Research Institute, 'The Open Distribution System Simulator (OpenDSS) ', [Online] Available: Electric Power Research Institute, http://sourceforge.net/projects/electricdss/, [Accessed: 29-Jun-2015].

[8] ENWL, 'ENA Smarter Networks Portal - Low Voltage Network Solutions'. [Online]. Available: http://www.smarternetworks.org/Project.aspx?ProjectID=404#downloads. [Accessed: 29-Jun-2015].

[9] I. Richardson, M. Thomson, D. Infield, and C. Clifford, 'Domestic electricity use: A high-resolution energy demand model', Energy and Buildings, vol. 42, no. 10, pp. 1878–1887, Oct. 2010.

[10] Simulink MathWorks United Kingdom, 'Implement three-phase transmission line section with lumped parameters'. [Online]. Available: http://uk.mathworks.com/help/physmod/sps/powersys/ref/threephasepisectionline.html. [Accessed: 19-Jan-2015].

Appendix

A1: Pulse Response Experiments' Results in Tabular Form

Table A1.1: Pulse Response Results for Initial Load of 10% during Summer

Size of Pulse	Soil Condition	Layer	0 min	15 min	30 min	45 min	60 min	75 min	90 min	105 min	120 min
25%	dry	Alu/XLPE	18.80	20.90	22.22	23.21	24.04	24.74	25.32	25.82	26.26
		Rubber/Alu	18.69	19.77	20.88	21.75	22.49	23.13	23.67	24.14	24.55
		PVC	18.68	19.67	20.75	21.60	22.33	22.96	23.49	23.95	24.36
	regular	Alu/XLPE	17.73	19.73	20.73	21.34	21.76	22.10	22.36	22.57	22.74
		Rubber/Alu	17.60	18.49	19.21	19.68	20.03	20.32	20.56	20.75	20.92
		PVC	17.59	18.37	19.05	19.51	19.85	20.13	20.36	20.55	20.72
	wet	Alu/XLPE	17.54	19.44	20.35	20.84	21.16	21.38	21.55	21.69	21.80
		Rubber/Alu	17.40	18.20	18.78	19.13	19.37	19.56	19.71	19.84	19.96
		PVC	17.38	18.07	18.61	18.94	19.18	19.36	19.51	19.64	19.75
50%	dry	Alu/XLPE	18.80	25.32	29.45	32.53	35.10	37.28	39.10	40.65	42.00
		Rubber/Alu	18.69	22.05	25.51	28.21	30.51	32.49	34.18	35.63	36.91
		PVC	18.68	21.76	25.13	27.78	30.04	32.00	33.66	35.10	36.37
	regular	Alu/XLPE	17.73	23.94	27.05	28.94	30.27	31.31	32.13	32.78	33.32
		Rubber/Alu	17.60	20.37	22.60	24.07	25.17	26.06	26.80	27.41	27.94
		PVC	17.59	20.04	22.15	23.56	24.63	25.50	26.22	26.82	27.35
	wet	Alu/XLPE	17.54	23.45	26.28	27.81	28.81	29.50	30.02	30.44	30.81
		Rubber/Alu	17.40	19.88	21.69	22.78	23.55	24.13	24.60	25.00	25.36
		PVC	17.38	19.54	21.22	22.25	22.99	23.55	24.01	24.40	24.76
100%	dry	Alu/XLPE	18.80	41.41	55.60	66.12	74.65	82.00	88.25	93.60	98.25
		Rubber/Alu	18.69	30.34	42.28	51.51	59.18	65.89	71.67	76.69	81.10
		PVC	18.68	29.38	41.01	50.06	57.61	64.23	69.95	74.92	79.29
	regular	Alu/XLPE	17.73	39.34	50.15	57.15	61.87	65.16	67.63	69.65	71.40
		Rubber/Alu	17.60	27.28	35.06	40.46	44.34	47.23	49.53	51.48	53.22
		PVC	17.59	26.15	33.53	38.71	42.49	45.32	47.59	49.52	51.25
	wet	Alu/XLPE	17.54	37.80	47.84	53.75	57.23	59.41	60.97	62.23	63.34
		Rubber/Alu	17.40	25.93	32.30	36.45	39.16	41.05	42.52	43.79	44.93
		PVC	17.38	24.81	30.71	34.62	37.22	39.07	40.53	41.77	42.91

Table A1.2: Pulse Response Results for Initial Load of 10% during Winter

Size of Pulse	Soil Condition	Layer	0 min	15 min	30 min	45 min	60 min	75 min	90 min	105 min	120 min
25%	dry	Alu/XLPE	9.80	11.90	13.22	14.21	15.04	15.74	16.32	16.82	17.26
		Rubber/Alu	9.69	10.77	11.88	12.75	13.49	14.13	14.67	15.14	15.55
		PVC	9.68	10.67	11.75	12.60	13.33	13.96	14.49	14.95	15.36
	regular	Alu/XLPE	8.73	10.73	11.73	12.34	12.76	13.10	13.36	13.57	13.74
		Rubber/Alu	8.60	9.49	10.21	10.68	11.03	11.32	11.56	11.75	11.92
		PVC	8.58	9.37	10.05	10.51	10.85	11.13	11.36	11.55	11.72
	wet	Alu/XLPE	8.54	10.44	11.35	11.84	12.16	12.38	12.55	12.69	12.80
		Rubber/Alu	8.40	9.20	9.77	10.13	10.37	10.56	10.71	10.84	10.96
		PVC	8.38	9.07	9.61	9.94	10.18	10.36	10.51	10.64	10.75
50%	dry	Alu/XLPE	9.80	16.32	20.45	23.53	26.10	28.28	30.10	31.65	33.00
		Rubber/Alu	9.69	13.05	16.51	19.21	21.51	23.49	25.18	26.63	27.91
		PVC	9.68	12.76	16.13	18.78	21.04	23.00	24.66	26.10	27.37
	regular	Alu/XLPE	8.73	14.94	18.05	19.94	21.27	22.31	23.13	23.78	24.32
		Rubber/Alu	8.60	11.37	13.60	15.07	16.17	17.06	17.80	18.41	18.94
		PVC	8.58	11.04	13.15	14.56	15.63	16.50	17.22	17.82	18.35
	wet	Alu/XLPE	8.54	14.45	17.28	18.81	19.81	20.50	21.02	21.44	21.81
		Rubber/Alu	8.40	10.88	12.69	13.78	14.55	15.13	15.60	16.00	16.36
		PVC	8.38	10.54	12.22	13.25	13.99	14.55	15.01	15.40	15.76
100%	dry	Alu/XLPE	9.80	32.41	46.60	57.12	65.65	73.00	79.25	84.60	89.25
		Rubber/Alu	9.69	21.34	33.28	42.51	50.18	56.89	62.67	67.69	72.10
		PVC	9.68	20.38	32.01	41.06	48.61	55.23	60.95	65.92	70.29
	regular	Alu/XLPE	8.73	30.34	41.15	48.15	52.87	56.16	58.63	60.65	62.40
		Rubber/Alu	8.60	18.28	26.06	31.46	35.34	38.23	40.53	42.48	44.22
		PVC	8.58	17.15	24.53	29.71	33.49	36.32	38.59	40.52	42.25
	wet	Alu/XLPE	8.54	28.80	38.84	44.75	48.23	50.41	51.97	53.23	54.34
		Rubber/Alu	8.40	16.93	23.30	27.45	30.16	32.05	33.52	34.79	35.93
		PVC	8.38	15.81	21.71	25.62	28.22	30.07	31.53	32.77	33.91

Table A1.3: Pulse Response Results for Initial Load of 25% during Summer

Size of Pulse	Soil Condition	Layer	0 min	15 min	30 min	45 min	60 min	75 min	90 min	105 min	120 min
25%	dry	Alu/XLPE	28.3	31.7	34.0	35.6	37.0	38.1	39.1	40.0	40.7
		Rubber/Alu	27.6	29.4	31.2	32.7	33.9	35.0	35.9	36.7	37.3
		PVC	27.5	29.1	30.9	32.4	33.6	34.6	35.5	36.3	37.0
	regular	Alu/XLPE	21.6	24.9	26.6	27.6	28.3	28.9	29.3	29.6	29.9
		Rubber/Alu	20.8	22.2	23.4	24.2	24.8	25.3	25.7	26.0	26.3
		PVC	20.7	22.0	23.1	23.9	24.4	24.9	25.3	25.6	25.9
	wet	Alu/XLPE	20.4	23.5	25.0	25.9	26.4	26.8	27.0	27.3	27.5
		Rubber/Alu	19.5	20.8	21.8	22.4	22.8	23.1	23.3	23.5	23.7
		PVC	19.4	20.5	21.4	22.0	22.4	22.7	22.9	23.1	23.3
50%	dry	Alu/XLPE	28.3	37.6	43.5	47.9	51.5	54.6	57.2	59.5	61.4
		Rubber/Alu	27.6	32.4	37.3	41.2	44.5	47.3	49.7	51.8	53.6
		PVC	27.5	31.9	36.7	40.5	43.7	46.5	48.9	50.9	52.7
	regular	Alu/XLPE	21.6	30.4	34.9	37.6	39.5	41.0	42.1	43.1	43.9
		Rubber/Alu	20.8	24.7	27.9	30.0	31.6	32.8	33.9	34.8	35.5
		PVC	20.7	24.1	27.2	29.2	30.7	32.0	33.0	33.8	34.6
	wet	Alu/XLPE	20.4	28.8	32.8	35.0	36.5	37.4	38.2	38.8	39.3
		Rubber/Alu	19.5	23.0	25.6	27.2	28.3	29.1	29.8	30.3	30.8
		PVC	19.4	22.5	24.8	26.3	27.4	28.2	28.8	29.4	29.9
100%	dry	Alu/XLPE	28.3	56.5	74.4	88.4	99.5	108.5	116.1	122.5	128.1
		Rubber/Alu	27.6	42.1	57.2	69.4	79.4	87.6	94.7	100.7	106.1
		PVC	27.5	40.8	55.5	67.4	77.3	85.5	92.4	98.4	103.7
	regular	Alu/XLPE	21.6	48.6	62.1	70.9	76.7	80.9	84.0	86.5	88.7
		Rubber/Alu	20.8	32.8	42.6	49.3	54.2	57.8	60.7	63.1	65.3
		PVC	20.7	31.4	40.6	47.1	51.8	55.3	58.1	60.6	62.7
	wet	Alu/XLPE	20.4	45.7	58.2	65.6	70.0	72.7	74.6	76.2	77.6
		Rubber/Alu	19.5	30.1	38.1	43.3	46.7	49.0	50.9	52.5	53.9
		PVC	19.4	28.6	36.0	40.9	44.2	46.5	48.3	49.9	51.3

Table A1.4: Pulse Response Results for Initial Load of 25% during Winter

Size of Pulse	Soil Condition	Layer	0 min	15 min	30 min	45 min	60 min	75 min	90 min	105 min	120 min
25%	dry	Alu/XLPE	19.3	22.7	25.0	26.6	28.0	29.1	30.1	31.0	31.7
		Rubber/Alu	18.6	20.4	22.2	23.7	24.9	26.0	26.9	27.7	28.3
		PVC	18.5	20.1	21.9	23.4	24.6	25.6	26.5	27.3	28.0
	regular	Alu/XLPE	12.6	15.9	17.6	18.6	19.3	19.9	20.3	20.6	20.9
		Rubber/Alu	11.8	13.2	14.4	15.2	15.8	16.3	16.7	17.0	17.3
		PVC	11.7	13.0	14.1	14.9	15.4	15.9	16.3	16.6	16.9
	wet	Alu/XLPE	11.4	14.5	16.0	16.9	17.4	17.8	18.0	18.3	18.5
		Rubber/Alu	10.5	11.8	12.8	13.4	13.8	14.1	14.3	14.5	14.7
		PVC	10.4	11.5	12.4	13.0	13.4	13.7	13.9	14.1	14.3
50%	dry	Alu/XLPE	19.3	28.6	34.5	38.9	42.5	45.6	48.2	50.5	52.4
		Rubber/Alu	18.6	23.4	28.3	32.2	35.5	38.3	40.7	42.8	44.6
		PVC	18.5	22.9	27.7	31.5	34.7	37.5	39.9	41.9	43.7
	regular	Alu/XLPE	12.6	21.4	25.9	28.6	30.5	32.0	33.1	34.1	34.9
		Rubber/Alu	11.8	15.7	18.9	21.0	22.6	23.8	24.9	25.8	26.5
		PVC	11.7	15.1	18.2	20.2	21.7	23.0	24.0	24.8	25.6
	wet	Alu/XLPE	11.4	19.8	23.8	26.0	27.5	28.4	29.2	29.8	30.3
		Rubber/Alu	10.5	14.0	16.6	18.2	19.3	20.1	20.8	21.3	21.8
		PVC	10.4	13.5	15.8	17.3	18.4	19.2	19.8	20.4	20.9
100%	dry	Alu/XLPE	19.3	47.5	65.4	79.4	90.5	99.5	107.1	113.5	119.1
		Rubber/Alu	18.6	33.1	48.2	60.4	70.4	78.6	85.7	91.7	97.1
		PVC	18.5	31.8	46.5	58.4	68.3	76.5	83.4	89.4	94.7
	regular	Alu/XLPE	12.6	39.6	53.1	61.9	67.7	71.9	75.0	77.5	79.7
		Rubber/Alu	11.8	23.8	33.6	40.3	45.2	48.8	51.7	54.1	56.3
		PVC	11.7	22.4	31.6	38.1	42.8	46.3	49.1	51.6	53.7
	wet	Alu/XLPE	11.4	36.7	49.2	56.6	61.0	63.7	65.6	67.2	68.6
		Rubber/Alu	10.5	21.1	29.1	34.3	37.7	40.0	41.9	43.5	44.9
		PVC	10.4	19.6	27.0	31.9	35.2	37.5	39.3	40.9	42.3

Table A1.5: Pulse Response Results for Initial Load of 50% during Summer

Size of Pulse	Soil Condition	Layer	0 min	15 min	30 min	45 min	60 min	75 min	90 min	105 min	120 min
25%	dry	Alu/XLPE	62.0	67.8	71.5	74.3	76.6	78.5	80.1	81.5	82.7
		Rubber/Alu	59.4	62.3	65.4	67.8	69.9	71.7	73.2	74.5	75.6
		PVC	58.9	61.7	64.7	67.0	69.1	70.8	72.3	73.6	74.7
	regular	Alu/XLPE	35.3	40.9	43.6	45.3	46.5	47.4	48.2	48.8	49.2
		Rubber/Alu	32.1	34.5	36.5	37.8	38.8	39.6	40.3	40.8	41.3
		PVC	31.6	33.8	35.7	36.9	37.9	38.7	39.3	39.9	40.3
	wet	Alu/XLPE	30.4	35.7	38.2	39.6	40.5	41.1	41.6	41.9	42.3
		Rubber/Alu	26.9	29.1	30.7	31.7	32.4	32.9	33.3	33.7	34.0
		PVC	26.5	28.4	29.9	30.8	31.5	32.0	32.4	32.7	33.1
50%	dry	Alu/XLPE	62.0	76.0	84.8	91.4	96.9	101.6	105.5	108.8	111.7
		Rubber/Alu	59.4	66.5	73.9	79.7	84.6	88.9	92.5	95.6	98.4
		PVC	58.9	65.5	72.7	78.4	83.3	87.4	91.0	94.1	96.8
	regular	Alu/XLPE	35.3	48.6	55.3	59.4	62.3	64.5	66.2	67.6	68.8
		Rubber/Alu	32.1	38.0	42.8	45.9	48.3	50.2	51.8	53.1	54.2
		PVC	31.6	36.9	41.4	44.4	46.7	48.6	50.1	51.4	52.5
	wet	Alu/XLPE	30.4	43.1	49.2	52.5	54.6	56.1	57.2	58.1	58.9
		Rubber/Alu	26.9	32.2	36.1	38.5	40.1	41.3	42.3	43.2	44.0
		PVC	26.5	31.1	34.7	36.9	38.5	39.7	40.7	41.5	42.3
100%	dry	Alu/XLPE	62.0	99.7	123.6	142.2	157.0	169.1	179.1	187.7	195.2
		Rubber/Alu	59.4	78.7	98.8	115.0	128.3	139.4	148.7	156.8	164.0
		PVC	58.9	76.7	96.3	112.2	125.3	136.2	145.4	153.4	160.5
	regular	Alu/XLPE	35.3	71.3	89.3	101.0	108.9	114.4	118.5	121.9	124.8
		Rubber/Alu	32.1	48.1	61.1	70.1	76.6	81.4	85.2	88.5	91.4
		PVC	31.6	45.8	58.1	66.8	73.1	77.8	81.6	84.8	87.7
	wet	Alu/XLPE	30.4	64.2	80.9	90.8	96.6	100.2	102.8	104.9	106.8
		Rubber/Alu	26.9	41.1	51.7	58.6	63.2	66.3	68.8	70.9	72.8
		PVC	26.5	38.8	48.7	55.2	59.5	62.6	65.0	67.1	69.0

Table A1.6: Pulse Response Results for Initial Load of 50% during Winter

Size of Pulse	Soil Condition	Layer	0 min	15 min	30 min	45 min	60 min	75 min	90 min	105 min	120 min
25%	dry	Alu/XLPE	53.0	58.8	62.5	65.3	67.6	69.5	71.1	72.5	73.7
		Rubber/Alu	50.4	53.3	56.4	58.8	60.9	62.7	64.2	65.5	66.6
		PVC	49.9	52.7	55.7	58.0	60.1	61.8	63.3	64.6	65.7
	regular	Alu/XLPE	26.3	31.9	34.6	36.3	37.5	38.4	39.2	39.8	40.2
		Rubber/Alu	23.1	25.5	27.5	28.8	29.8	30.6	31.3	31.8	32.3
		PVC	22.6	24.8	26.7	27.9	28.9	29.7	30.3	30.9	31.3
	wet	Alu/XLPE	21.4	26.7	29.2	30.6	31.5	32.1	32.6	32.9	33.3
		Rubber/Alu	17.9	20.1	21.7	22.7	23.4	23.9	24.3	24.7	25.0
		PVC	17.5	19.4	20.9	21.8	22.5	23.0	23.4	23.7	24.1
50%	dry	Alu/XLPE	53.0	67.0	75.8	82.4	87.9	92.6	96.5	99.8	102.7
		Rubber/Alu	50.4	57.5	64.9	70.7	75.6	79.9	83.5	86.6	89.4
		PVC	49.9	56.5	63.7	69.4	74.3	78.4	82.0	85.1	87.8
	regular	Alu/XLPE	26.3	39.6	46.3	50.4	53.3	55.5	57.2	58.6	59.8
		Rubber/Alu	23.1	29.0	33.8	36.9	39.3	41.2	42.8	44.1	45.2
		PVC	22.6	27.9	32.4	35.4	37.7	39.6	41.1	42.4	43.5
	wet	Alu/XLPE	21.4	34.1	40.2	43.5	45.6	47.1	48.2	49.1	49.9
		Rubber/Alu	17.9	23.2	27.1	29.5	31.1	32.3	33.3	34.2	35.0
		PVC	17.5	22.1	25.7	27.9	29.5	30.7	31.7	32.5	33.3
100%	dry	Alu/XLPE	53.0	90.7	114.6	133.2	148.0	160.1	170.1	178.7	186.2
		Rubber/Alu	50.4	69.7	89.8	106.0	119.3	130.4	139.7	147.8	155.0
		PVC	49.9	67.7	87.3	103.2	116.3	127.2	136.4	144.4	151.5
	regular	Alu/XLPE	26.3	62.3	80.3	92.0	99.9	105.4	109.5	112.9	115.8
		Rubber/Alu	23.1	39.1	52.1	61.1	67.6	72.4	76.2	79.5	82.4
		PVC	22.6	36.8	49.1	57.8	64.1	68.8	72.6	75.8	78.7
	wet	Alu/XLPE	21.4	55.2	71.9	81.8	87.6	91.2	93.8	95.9	97.8
		Rubber/Alu	17.9	32.1	42.7	49.6	54.2	57.3	59.8	61.9	63.8
		PVC	17.5	29.8	39.7	46.2	50.5	53.6	56.0	58.1	60.0

Table A1.7: Pulse Response Results for Initial Load of 100% during Summer

Size of Pulse	Soil Condition	Layer	0 min	15 min	30 min	45 min	60 min	75 min	90 min	105 min	120 min
25%	dry	Alu/XLPE	197.0	207.5	214.1	219.1	223.2	226.7	229.6	232.1	234.3
		Rubber/Alu	186.4	191.8	197.4	201.7	205.4	208.6	211.3	213.6	215.7
		PVC	184.8	189.7	195.1	199.3	203.0	206.1	208.8	211.1	213.1
	regular	Alu/XLPE	90.3	100.3	105.3	108.3	110.4	112.1	113.4	114.5	115.3
		Rubber/Alu	77.2	81.7	85.3	87.6	89.4	90.8	92.0	93.0	93.8
		PVC	75.5	79.4	82.8	85.1	86.8	88.2	89.3	90.3	91.2
	wet	Alu/XLPE	70.6	80.1	84.7	87.1	88.7	89.8	90.7	91.4	91.9
		Rubber/Alu	56.6	60.6	63.5	65.3	66.5	67.4	68.2	68.8	69.4
		PVC	54.9	58.3	61.0	62.7	63.9	64.8	65.5	66.1	66.7
50%	dry	Alu/XLPE	197.0	220.3	235.0	246.0	255.2	263.0	269.5	275.0	279.9
		Rubber/Alu	186.4	198.4	210.7	220.4	228.6	235.6	241.7	246.9	251.4
		PVC	184.8	195.7	207.7	217.2	225.3	232.2	238.2	243.3	247.9
	regular	Alu/XLPE	90.3	112.8	123.9	130.6	135.3	138.9	141.8	144.1	146.0
		Rubber/Alu	77.2	87.3	95.3	100.5	104.3	107.5	110.1	112.3	114.2
		PVC	75.5	84.4	91.9	96.9	100.7	103.8	106.3	108.5	110.3
	wet	Alu/XLPE	70.6	91.7	102.2	108.3	112.0	114.2	115.9	117.2	118.3
		Rubber/Alu	56.6	65.5	72.1	76.4	79.3	81.2	82.8	84.1	85.3
		PVC	54.9	62.6	68.7	72.8	75.5	77.4	78.9	80.2	81.4
100%	dry	Alu/XLPE	197.0	253.5	289.4	317.3	339.5	357.6	372.6	385.5	396.8
		Rubber/Alu	186.4	215.4	245.5	269.9	289.8	306.4	320.4	332.5	343.3
		PVC	184.8	211.4	240.7	264.6	284.2	300.6	314.4	326.5	337.1
	regular	Alu/XLPE	90.3	144.7	171.5	188.4	200.3	208.6	214.9	220.0	224.4
		Rubber/Alu	77.2	101.8	120.9	134.0	143.7	151.0	156.8	161.8	166.2
		PVC	75.5	97.2	115.4	127.9	137.4	144.5	150.2	155.1	159.5
	wet	Alu/XLPE	70.6	123.2	147.2	160.8	169.6	175.1	179.1	182.3	185.1
		Rubber/Alu	56.6	78.8	94.2	104.0	110.8	115.5	119.3	122.5	125.4
		PVC	54.9	74.2	88.5	97.7	104.2	108.8	112.6	115.7	118.6

Table A1.8: Pulse Response Results for Initial Load of 100% during Winter

Size of Pulse	Soil Condition	Layer	0 min	15 min	30 min	45 min	60 min	75 min	90 min	105 min	120 min
25%	dry	Alu/XLPE	188.0	198.5	205.1	210.1	214.2	217.7	220.6	223.1	225.3
		Rubber/Alu	177.4	182.8	188.4	192.7	196.4	199.6	202.3	204.6	206.7
		PVC	175.8	180.7	186.1	190.3	194.0	197.1	199.8	202.1	204.1
	regular	Alu/XLPE	81.3	91.3	96.3	99.3	101.4	103.1	104.4	105.5	106.3
		Rubber/Alu	68.2	72.7	76.3	78.6	80.4	81.8	83.0	84.0	84.8
		PVC	66.5	70.4	73.8	76.1	77.8	79.2	80.3	81.3	82.2
	wet	Alu/XLPE	61.6	71.1	75.7	78.1	79.7	80.8	81.7	82.4	82.9
		Rubber/Alu	47.6	51.6	54.5	56.3	57.5	58.4	59.2	59.8	60.4
		PVC	45.9	49.3	52.0	53.7	54.9	55.8	56.5	57.1	57.7
50%	dry	Alu/XLPE	188.0	211.3	226.0	237.0	246.2	254.0	260.5	266.0	270.9
		Rubber/Alu	177.4	189.4	201.7	211.4	219.6	226.6	232.7	237.9	242.4
		PVC	175.8	186.7	198.7	208.2	216.3	223.2	229.2	234.3	238.9
	regular	Alu/XLPE	81.3	103.8	114.9	121.6	126.3	129.9	132.8	135.1	137.0
		Rubber/Alu	68.2	78.3	86.3	91.5	95.3	98.5	101.1	103.3	105.2
		PVC	66.5	75.4	82.9	87.9	91.7	94.8	97.3	99.5	101.3
	wet	Alu/XLPE	61.6	82.7	93.2	99.3	103.0	105.2	106.9	108.2	109.3
		Rubber/Alu	47.6	56.5	63.1	67.4	70.3	72.2	73.8	75.1	76.3
		PVC	45.9	53.6	59.7	63.8	66.5	68.4	69.9	71.2	72.4
100%	dry	Alu/XLPE	188.0	244.5	280.4	308.3	330.5	348.6	363.6	376.5	387.8
		Rubber/Alu	177.4	206.4	236.5	260.9	280.8	297.4	311.4	323.5	334.3
		PVC	175.8	202.4	231.7	255.6	275.2	291.6	305.4	317.5	328.1
	regular	Alu/XLPE	81.3	135.7	162.5	179.4	191.3	199.6	205.9	211.0	215.4
		Rubber/Alu	68.2	92.8	111.9	125.0	134.7	142.0	147.8	152.8	157.2
		PVC	66.5	88.2	106.4	118.9	128.4	135.5	141.2	146.1	150.5
	wet	Alu/XLPE	61.6	114.2	138.2	151.8	160.6	166.1	170.1	173.3	176.1
		Rubber/Alu	47.6	69.8	85.2	95.0	101.8	106.5	110.3	113.5	116.4
		PVC	45.9	65.2	79.5	88.7	95.2	99.8	103.6	106.7	109.6

A2: Scatter Plots of Cable Temperature

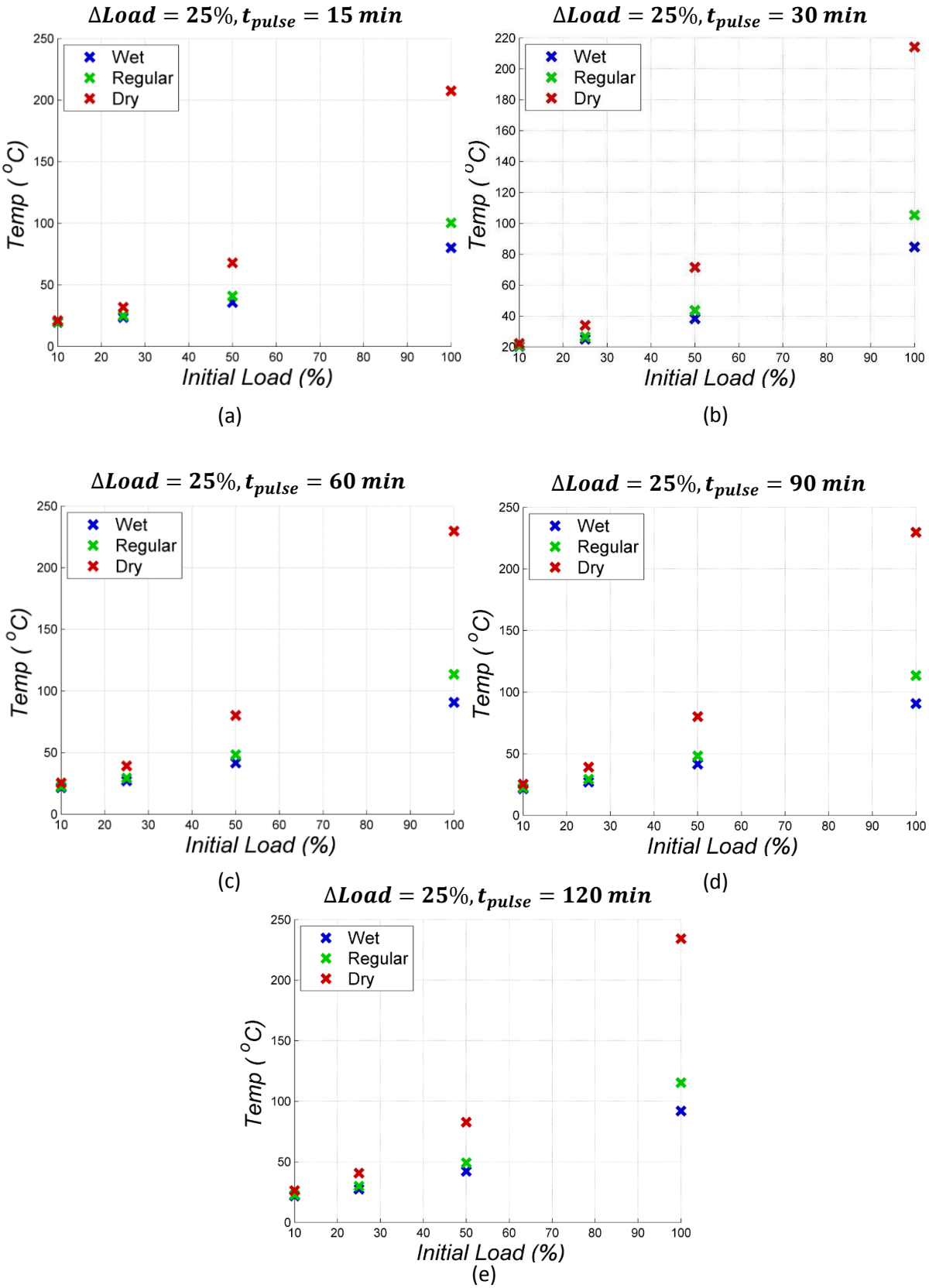

Figure A2.1: Pulse Response Results for $\Delta Load = 25\%$ during Summer

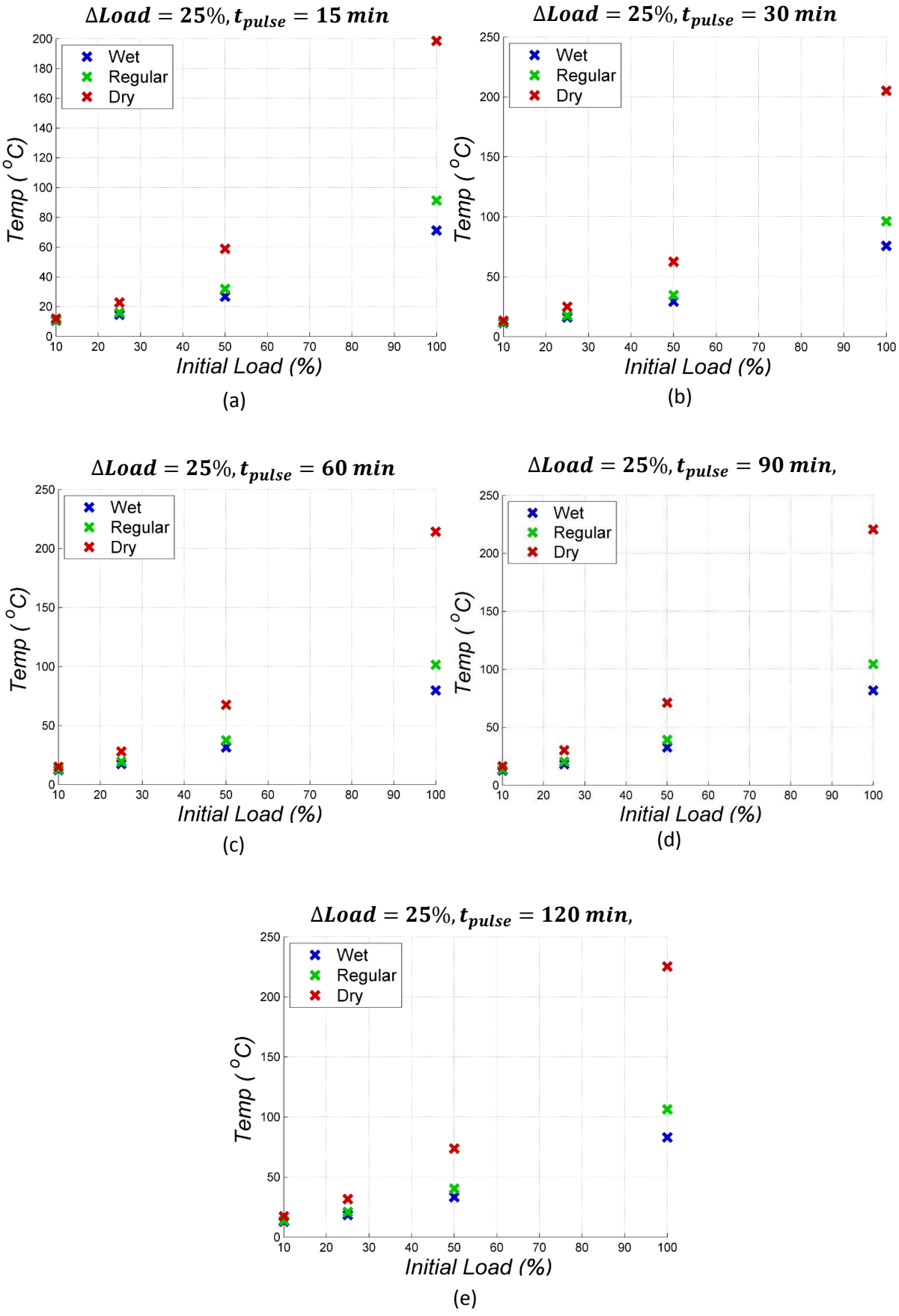

Figure A2.2: Pulse Response Results for $\Delta Load = 25\%$ during Winter

$\Delta Load = 50\%, t_{pulse} = 15\ min$

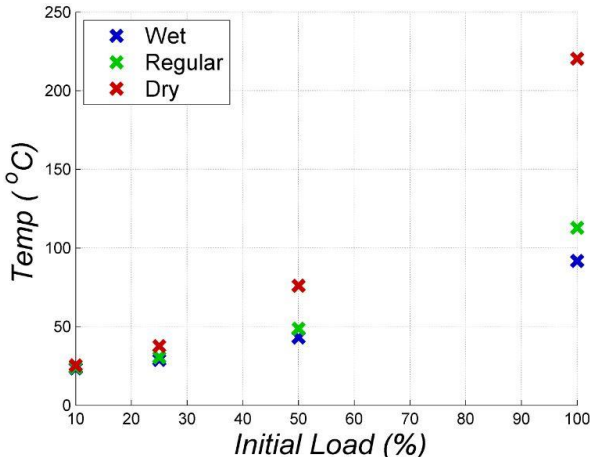

(a)

$\Delta Load = 50\%, t_{pulse} = 30\ min$

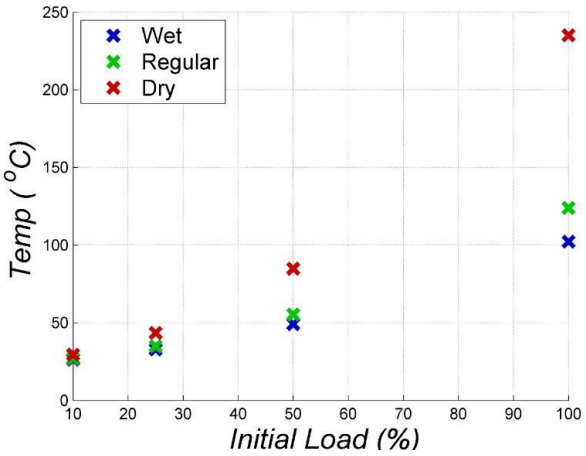

(b)

$\Delta Load = 50\%, t_{pulse} = 60\ min$

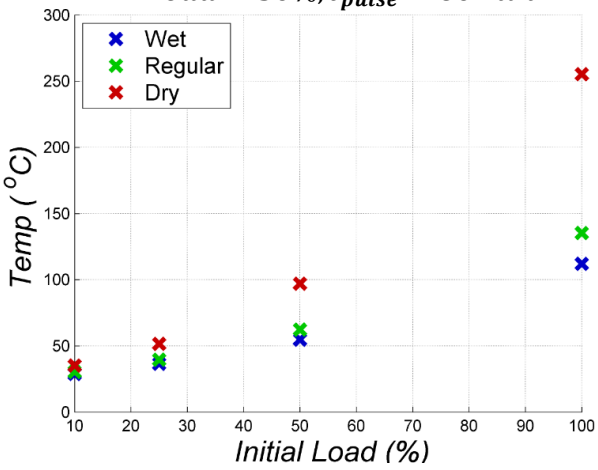

(c)

$\Delta Load = 50\%, t_{pulse} = 90\ min,$

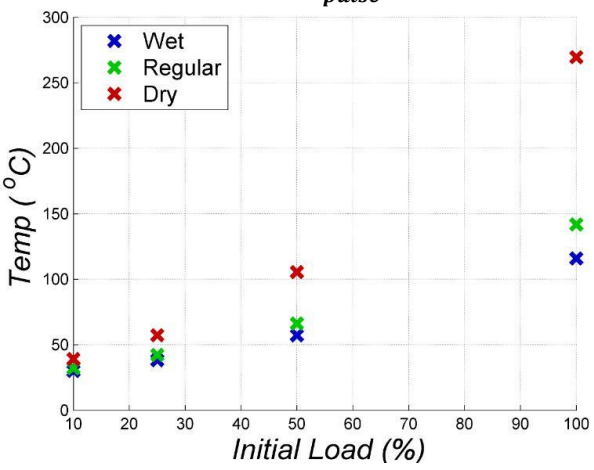

(d)

$\Delta Load = 50\%, t_{pulse} = 120\ min,$

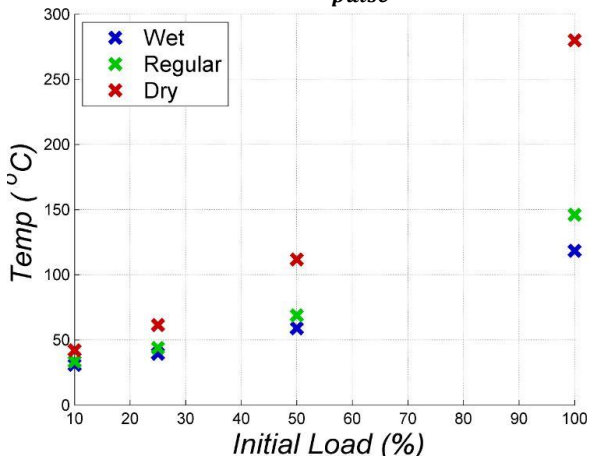

(e)

Figure A2.3: Pulse Response Results for $\Delta Load = 50\%$ during Summer

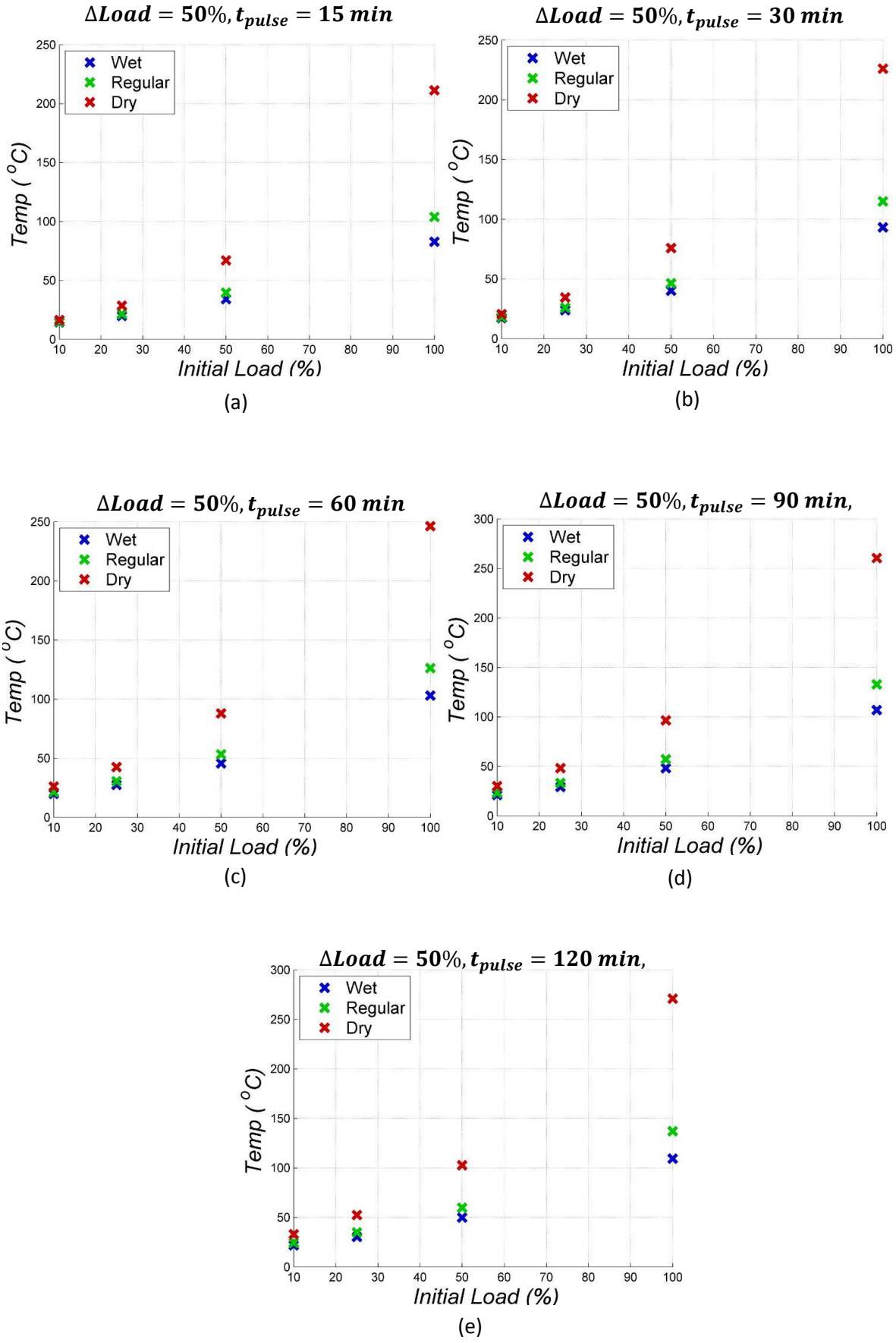

Figure A2.4: Pulse Response Results for $\Delta Load = 50\%$ during Winter

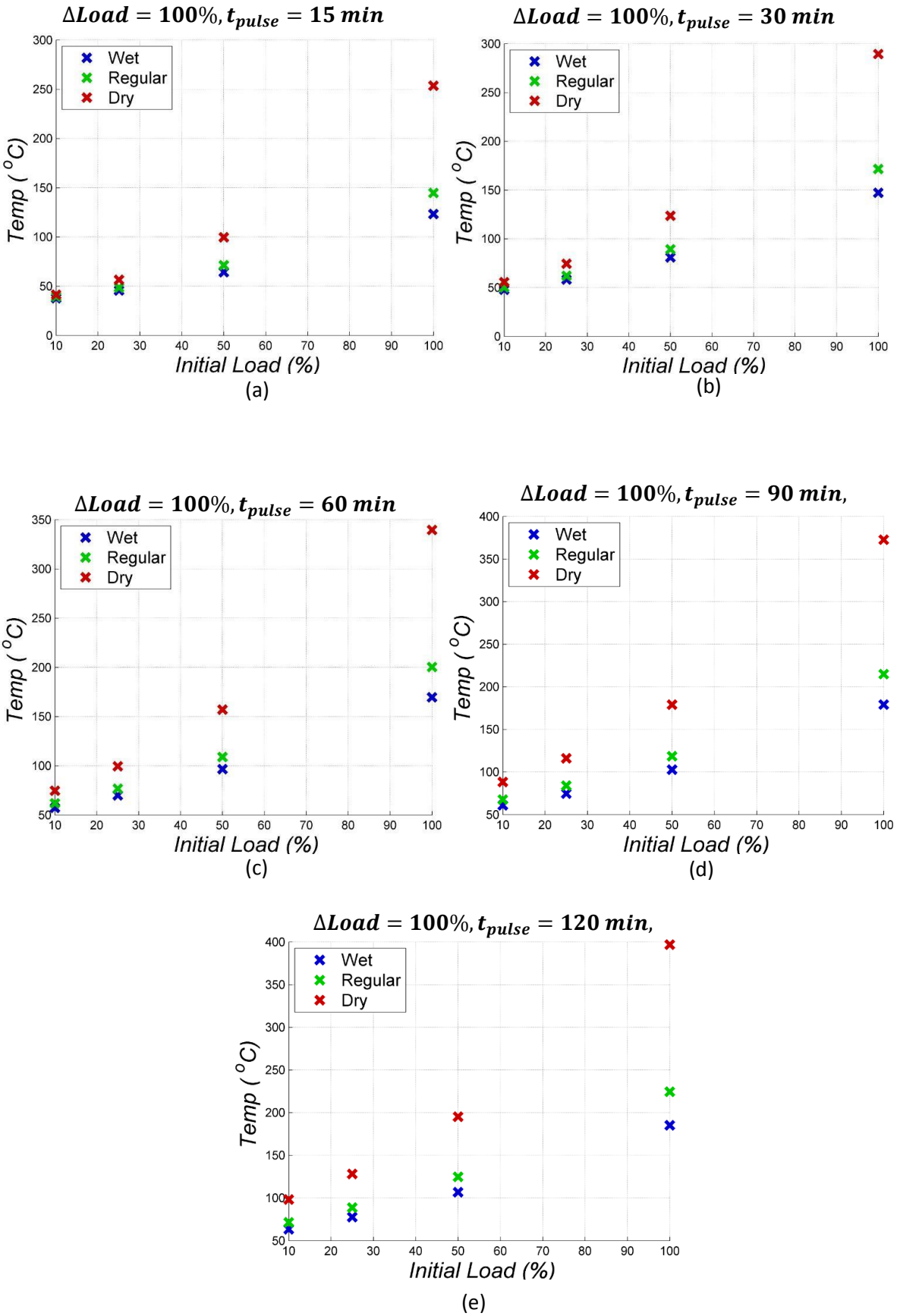

Figure A2.5: Pulse Response Results for $\Delta Load = 100\%$ during Summer

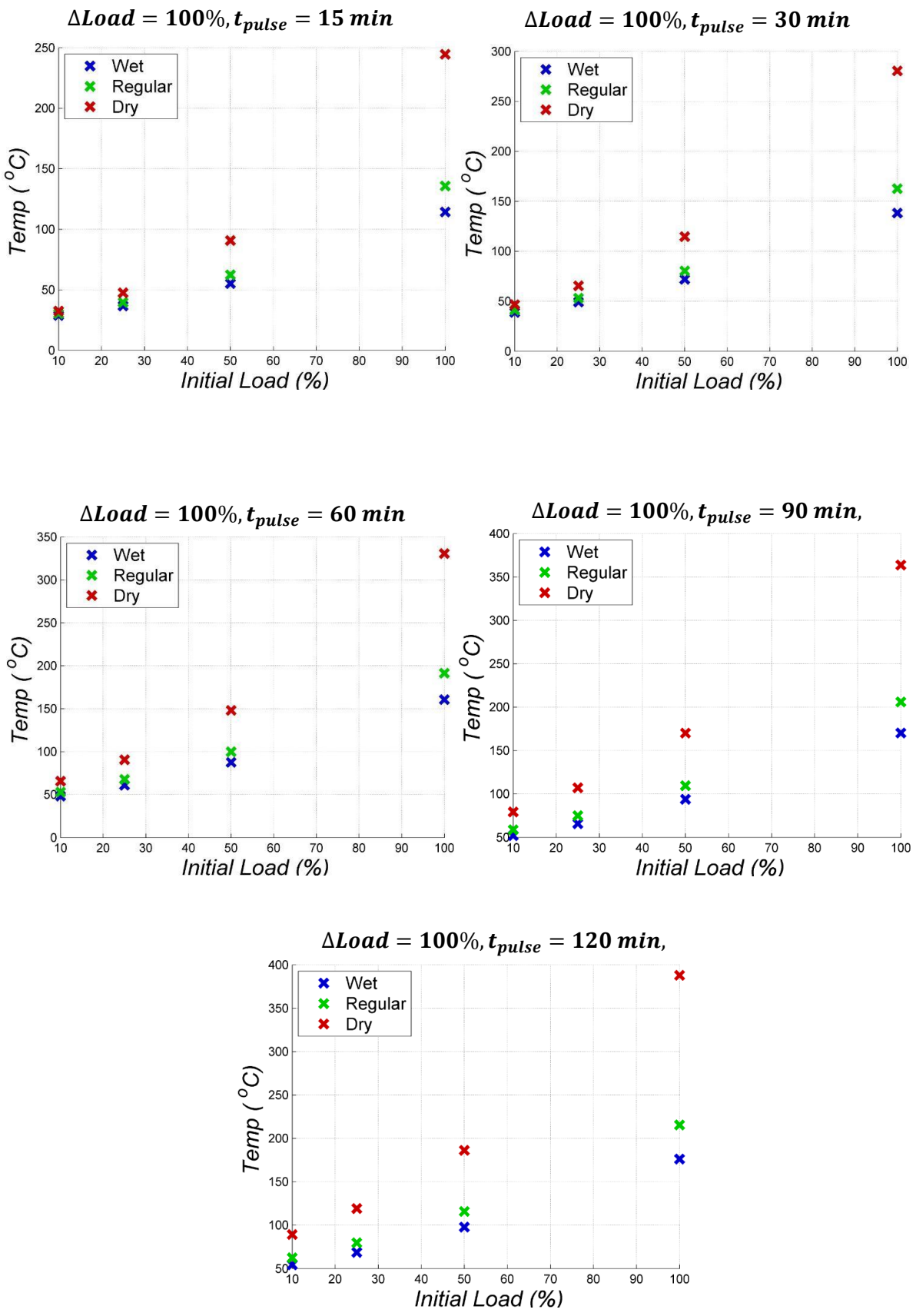

Figure A2.6: Pulse Response Results for $\Delta Load = 100\%$ during Winter

A3: Worst Case and Best Case Scenario Pulse Response Plots of Cable Temperature

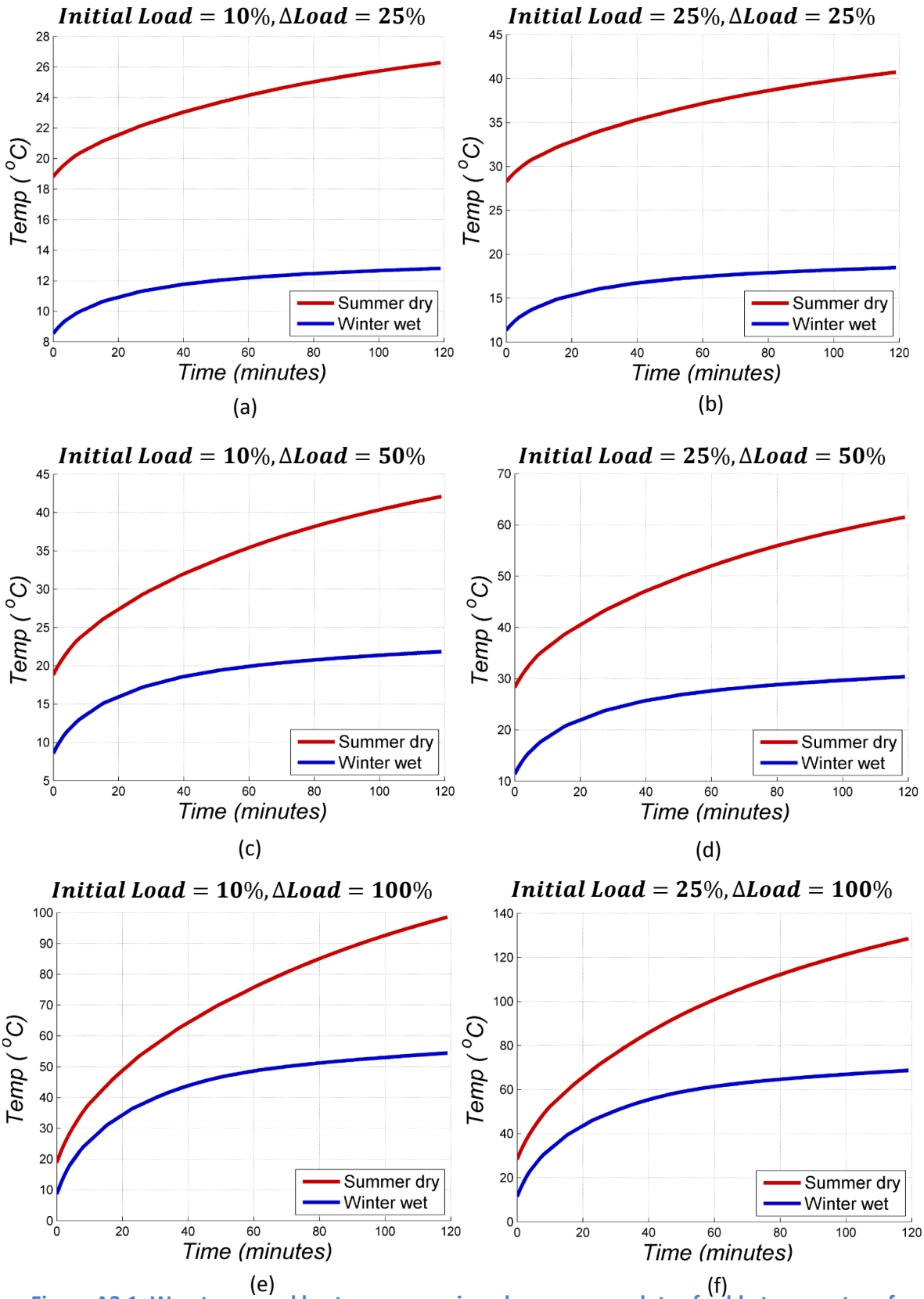

Figure A3.1: Worst case and best case scenario pulse response plots of cable temperature for initial load of 10% and initial load of 25%

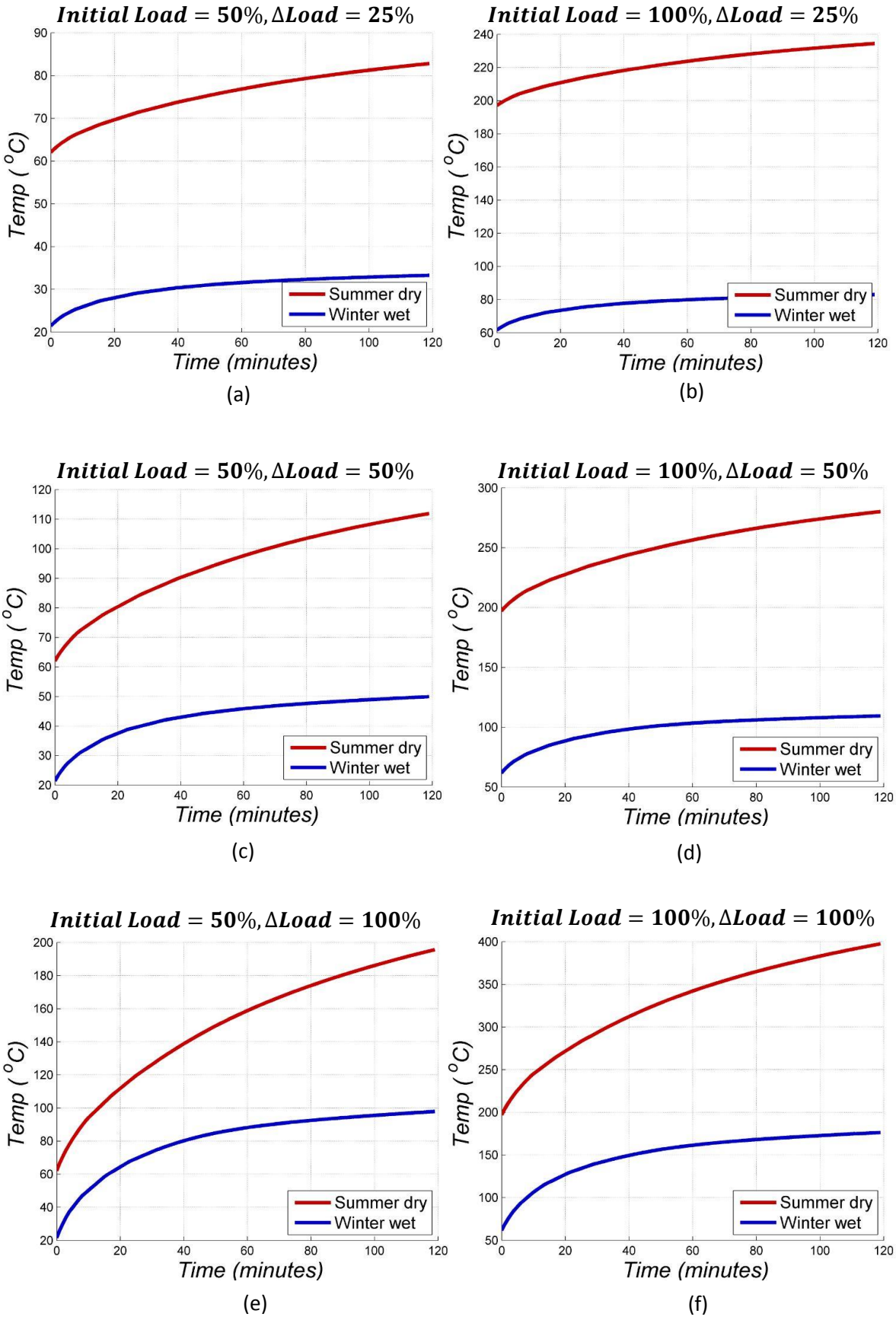

Figure A3.2: Worst case and best case scenario pulse response plots of cable temperature for initial load of 50% and initial load of 100%

A4: Algebraic Equations Describing Simplified Thermal Model

Algebraic equations describing the relationship between cable temperature (Alu/XLPE layer) and the initial cable loading, step change in cable loading and ambient temperature are given as follows.

For dry soil condition:

$$T(15\text{min}) = 0.018 \cdot Load_0^2 + 0.0037 \cdot Load_0 \cdot \Delta Load + 0.0019 \cdot \Delta Load^2 + T_A$$

$$T(30\text{min}) = 0.018 \cdot Load_0^2 + 0.0059 \cdot Load_0 \cdot \Delta Load + 0.0031 \cdot \Delta Load^2 + T_A$$

$$T(45\text{min}) = 0.018 \cdot Load_0^2 + 0.0074 \cdot Load_0 \cdot \Delta Load + 0.0039 \cdot \Delta Load^2 + T_A$$

$$T(60\text{min}) = 0.018 \cdot Load_0^2 + 0.0087 \cdot Load_0 \cdot \Delta Load + 0.0046 \cdot \Delta Load^2 + T_A$$

$$T(75\text{min}) = 0.018 \cdot Load_0^2 + 0.0100 \cdot Load_0 \cdot \Delta Load + 0.0052 \cdot \Delta Load^2 + T_A$$

$$T(90\text{min}) = 0.018 \cdot Load_0^2 + 0.0112 \cdot Load_0 \cdot \Delta Load + 0.0057 \cdot \Delta Load^2 + T_A$$

$$T(105\text{min}) = 0.018 \cdot Load_0^2 + 0.0122 \cdot Load_0 \cdot \Delta Load + 0.0062 \cdot \Delta Load^2 + T_A$$

$$T(120\text{min}) = 0.018 \cdot Load_0^2 + 0.0130 \cdot Load_0 \cdot \Delta Load + 0.0066 \cdot \Delta Load^2 + T_A$$

For regular soil moisture condition:

$$T(15\text{min}) = 0.0073 \cdot Load_0^2 + 0.0034 \cdot Load_0 \cdot \Delta Load + 0.0018 \cdot \Delta Load^2 + T_A$$

$$T(30\text{min}) = 0.0073 \cdot Load_0^2 + 0.0051 \cdot Load_0 \cdot \Delta Load + 0.0027 \cdot \Delta Load^2 + T_A$$

$$T(45\text{min}) = 0.0073 \cdot Load_0^2 + 0.0062 \cdot Load_0 \cdot \Delta Load + 0.0033 \cdot \Delta Load^2 + T_A$$

$$T(60\text{min}) = 0.0073 \cdot Load_0^2 + 0.007 \cdot Load_0 \cdot \Delta Load + 0.0038 \cdot \Delta Load^2 + T_A$$

$$T(75\text{min}) = 0.0073 \cdot Load_0^2 + 0.0077 \cdot Load_0 \cdot \Delta Load + 0.0040 \cdot \Delta Load^2 + T_A$$

$$T(90\text{min}) = 0.0073 \cdot Load_0^2 + 0.0081 \cdot Load_0 \cdot \Delta Load + 0.0042 \cdot \Delta Load^2 + T_A$$

$$T(105\text{min}) = 0.0073 \cdot Load_0^2 + 0.0086 \cdot Load_0 \cdot \Delta Load + 0.0043 \cdot \Delta Load^2 + T_A$$

$$T(120\text{min}) = 0.0073 \cdot Load_0^2 + 0.0089 \cdot Load_0 \cdot \Delta Load + 0.0045 \cdot \Delta Load^2 + T_A$$

For wet soil moisture condition:

$$T(15\text{min}) = 0.0054 \cdot Load_0^2 + 0.0036 \cdot Load_0 \cdot \Delta Load + 0.0017 \cdot \Delta Load^2 + T_A$$

$$T(30\text{min}) = 0.0054 \cdot Load_0^2 + 0.0050 \cdot Load_0 \cdot \Delta Load + 0.0026 \cdot \Delta Load^2 + T_A$$

$$T(45\text{min}) = 0.0054 \cdot Load_0^2 + 0.0054 \cdot Load_0 \cdot \Delta Load + 0.0031 \cdot \Delta Load^2 + T_A$$

$$T(60\text{min}) = 0.0054 \cdot Load_0^2 + 0.0060 \cdot Load_0 \cdot \Delta Load + 0.0033 \cdot \Delta Load^2 + T_A$$

$$T(75\text{min}) = 0.0054 \cdot Load_0^2 + 0.0065 \cdot Load_0 \cdot \Delta Load + 0.0035 \cdot \Delta Load^2 + T_A$$

$$T(90\text{min}) = 0.0054 \cdot Load_0^2 + 0.0068 \cdot Load_0 \cdot \Delta Load + 0.0036 \cdot \Delta Load^2 + T_A$$

$$T(105\text{min}) = 0.0054 \cdot Load_0^2 + 0.0072 \cdot Load_0 \cdot \Delta Load + 0.0037 \cdot \Delta Load^2 + T_A$$

$$T(120\text{min}) = 0.0054 \cdot Load_0^2 + 0.0075 \cdot Load_0 \cdot \Delta Load + 0.0038 \cdot \Delta Load^2 + T_A$$

where $T(x)$ denotes cable temperature at time x, $Load_0$ denotes initial load expressed as percentage of the rated cable current (335A per phase), $\Delta Load$ denotes the step change of cable loading during the pulse expressed as percentage of the rated cable current (335A per phase) and T_A denotes ambient temperature.